MODELING OF PORE FORMATION IN POROUS MATERIALS

A Thesis Submitted to
the Graduate School of Engineering and Sciences of
İzmir Institute of Technology
in Partial Fulfillment of the Requirements for the Degree of

MASTER OF SCIENCE

in Materials Science and Engineering

by
Sevkan ÜLKER

July 2017
İZMİR

We approve the thesis of **Sevkan ÜLKER**

Examining Committee Members:

Prof. Dr. Mustafa GÜDEN
Department of Mechanical Engineering, Izmir Institute of Technology

Prof. Dr. Mustafa Muammer DEMİR
Department of Materials Science and Engineering, Izmir Institute of Technology

Prof. Dr. Ali Aydın GÖKTAŞ
Department of Metallurgical and Materials Engineering, Dokuz Eylul University

20 July 2017

Prof. Dr. Mustafa GÜDEN
Supervisor, Department of Mechanical Engineering
Izmir Institute of Technology

Asst. Prof. Dr. Yaşar AKDOĞAN
Co-Supervisor, Department of Materials Science and Engineering
Izmir Institute of Technology

Prof. Dr. Mustafa M. DEMİR
Head of the Department of Materials Science and Engineering

Prof. Dr. Aysun SOFUĞLU
Dean of the Graduated School of Engineering and Sciences

ACKNOWLEDGEMENTS

I would like to thank my prior advisor Asst. Prof. Dr. Ufuk ŞENTÜRK, and my advisor Prof. Dr. Mustafa GÜDEN for their guidance on my thesis study as well as the endless support they have provided during the course of my thesis. I have learned not only the whole theory, material science, glass science and experimental techniques, but also the value of assiduity, and the virtue of being honest. I want to thank for their understanding, constant invaluable guidance, encouragement, motivation, incredible support, and immense knowledge at every stage of my thesis study. I feel lucky to be able to work with them, learn from them, and am proud of being one of their students.

Besides my advisor, I would like to thank the other members of my thesis committee for their encouragement and insightful comments.

My wonderful wife, Pınar ÇETİN ÜLKER, has always been with me every step of the way, and I'd like to express my heartfelt gratitude for her unconditional love, support, encouragement, and instilling in me the belief that I could do anything I put my mind to.

Thanks to my dear family, Emel ÖZKURAL and Metin ÖZKURAL for their support and encouragement.

Lastly, thanks also to Doğuş ZEREN and Ümmü Gülsüm SEZİŞ for their warm friendship and technical support.

ABSTRACT

MODELING OF PORE FORMATION IN POROUS MATERIALS

The purpose of this thesis is to model the expansion behavior of aqueous slurries. Foamed or cellular material made using such method is known, especially in the concrete industry. What appears to be lacking in the literature is the knowledge of pore formation and pore growth in inorganic particles based on aqueous slurry systems that result in the formation of cellular structures. The motivation of this study is to provide a scientific view in identifying and explaining the critical parameters that govern the pore growth and expansion of such slurry based systems. Bubble growth and pore formation are also studied experimentally. Experimental results are used to compare with the empirical study conducted by Kanehira at al. (Kanehira, et al., 2013), and mathematical modeling of pore formation plotted with Wolfram Mathematica software. Experimental procedure consists of three types of aluminum and calcium ratios which provide information about bubble growth and pore formation. These types are 50% aluminum – 50% calcium hydroxide (50/50), 70% aluminum – 30% calcium hydroxide (70/30), and 80% aluminum – 20% calcium hydroxide (80/20).

According to the results of studies, mathematical modeling system consists of the pressure difference between the inside and outside of a spherical bubble as the driving force for defining growth. While aluminum ratio increases, bubble growth rate decreases due to release of hydrogen gases which affect bubble expansion phenomenon. In the experimental and mathematical modeling, 50/50 ratio has maximum bubble growth rate compared to 70/30 and 80/20 ratios. The results of experimental and mathematical modeling suggest that viscosity is a very significant parameter which controls the bubble growth rate.

ÖZET

GÖZENEKLİ MALZEMELERDE GÖZENEK OLUŞUMUNUN MODELLENMESİ

Bu tezin amacı, sulu çamurların genişleme davranışını modellemektir. Köpüklü veya hücresel malzeme, özellikle beton endüstrisinde bu yöntem kullanılarak yapılmış olduğu bilinmektedir. Literatürde eksik olan şey, hücre yapılarının oluşumuyla sonuçlanan sulu çamur sistemlerine dayanan inorganik parçacıkta gözenek oluşumu ve gözenek büyümesinin bilgisidir. Bu çalışmanın amacı, çamur esaslı sistemlerin gözenek büyümesini ve genişlemesini yöneten kritik parametrelerin tanımlanmasında ve açıklanmasında bilimsel bir görüş sağlamaktır. Kabarcık büyümesi ve gözenek oluşumu ayrıca deneysel olarak incelenmiştir. Deneysel sonuçlar, Kanehira ve arkadaşları tarafından yürütülen deneysel çalışma ve Wolfram Mathematica yazılımı ile çizilen gözenek oluşumunun matematiksel modellenmesi karşılaştırmak için kullanılmıştır. Deney prosedürü, kabarcık büyümesi ve gözenek oluşumu hakkında bilgi veren üç tip alüminyum ve kalsiyum oranını içerir. Bu tipler %50 alüminyum- %50 kalsiyum hidroksit (50/50), %70 alüminyum- %30 kalsiyum hidroksit (70/30) ve %80 alüminyum- %20 kalsiyum hidroksittir (80/20).

Bu çalışmanın sonuçları; matematiksel modelleme sistemi, büyümeyi tanımlamak için itici güç olarak küresel bir kabarcığın içi ve dışı arasındaki basınç farkını içerir. Alüminyum oranı arttıkça, kabarcık oluşma hızı, kabarcık genişleme olgusunu etkileyen hidrojen gazlarının salınmasına bağlı olarak azalır. Deneysel ve matematiksel modellemede 50/50 oranı, 70/30 ve 80/20 oranlarına göre maksimum kabarcık büyüme oranına sahiptir. Deneysel ve matematiksel olarak, viskozite, kabarcık büyüme oranını kontrol eden çok önemli bir parametredir.

To my Wife…

TABLE OF CONTENTS

LIST OF FIGURES

Figure **Page**

LIST OF TABLES

Table **Page**

LIST OF ABBREVIATIONS

AAC……Autoclaved Aerated Concrete

NAAC……..Non-Autoclaved Aerated Concrete

PC……...Pulverized Coal

FBC……..Fluidized-Bed Combustion

CMC……...Carboxymethyl Cellulose

PCC.....Portland Cement Concrete

DI.....Deionized

CHAPTER 1

INTRODUCTION

The materials containing a gas or air in their solid structure are called porous solids. The presence of air gives the solid materials lightness as well as other important mechanical and physical properties such as low thermal conductivity. Porous solids serve as structural bodies in nature such aswood and bone. While man-made porous materials are designed much more functionally rather than structurally, and widely used in energy management, vibration suppression, heat insulation, sound absorption and fluid filtration (Liu & Chen, First Edition 2014).

One of the important features of porous materials is that they contain many pores. The pores are in fact intentionally introduced in order to give certain functionality to the material. Therefore, the materials containing unintentional pores, i.e. defects, such as few holes and crannies which reduce the material performance are not considered porous. A porous material must contain certain numbers of pores that are sufficient to achieve the expected performance index. Depending on the number of pores, the porous materials can be classified as low, medium and high porosity. The pores are usually closed in a typical low and medium porosity material, as seen in Figure 1.1. The closed pores act like impure phase in the structure. Depending on the pore morphology and continuous solid phase, classification of high porosity materials may change. First of all the continuous solid has a two dimensional array of polygons; the pores are isolated in space, taking on polygonal columniations; and the shape of pore is triangle, quadrangle, or hexagon. These materials are called honeycombs (Figure 1.2). If the continuous solid has a three-dimensional reticulated structure, then the resultant structure is called three-dimensional reticulated foam (Figure 1.3). In reticulated foams, the pores are connective; therefore, they have a typical open cell structure. The continuous solid displays the cell wall structure and the pores may be in spherical or polyhedron shape (Figure 1.4). Such three-dimensional porous materials are called bubble foamed materials. The cell wall may separate many isolated closed pores or cells, forming a closed cell, bubble like foamed substance. In the literature, three-dimensional reticulated foamed materials are referred to as open cell foamed materials;

closed cell, bubble like foamed materials are called closed cell foamed materials; and open cell, bubble like foamed materials are half open cell foamed materials.

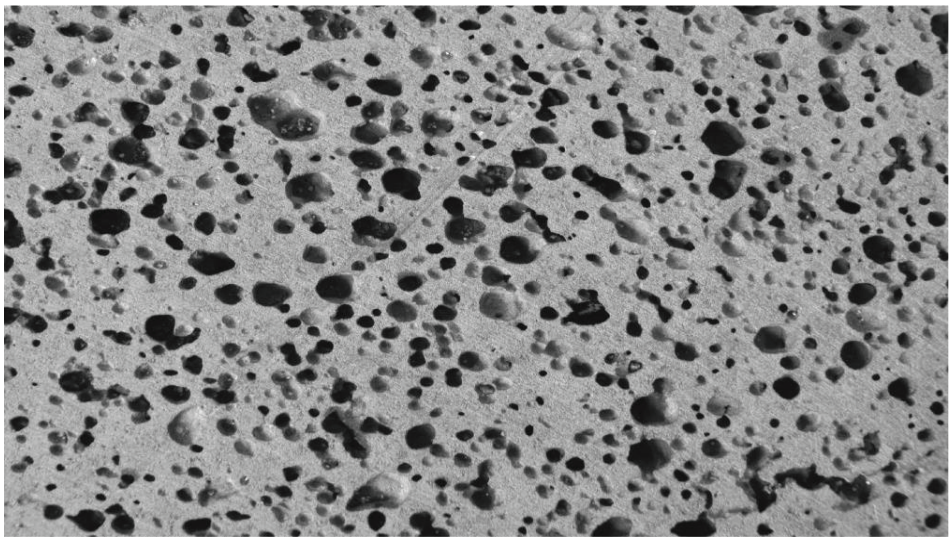

Figure 1.1. Porous composite oxide ceramics, which is a low porosity material, shown as a cross-sectional image. (Source: LIU & CHEN, First Edition 2014)

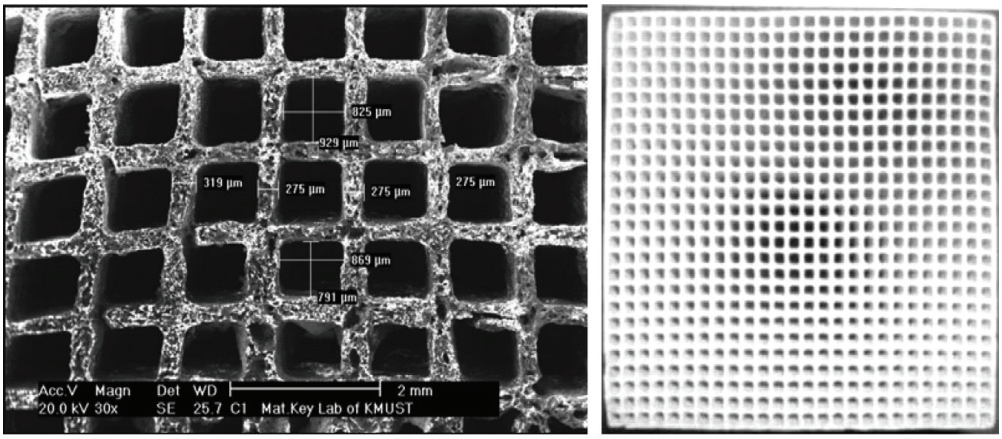

Figure 1.2. Two-dimensional honeycomb materials: (a) conductive honeycomb ceramics with quasi-square pores; (b) thermal storage of honeycomb ceramics with square pores (Source: Liu & Chen, First Edition 2014)

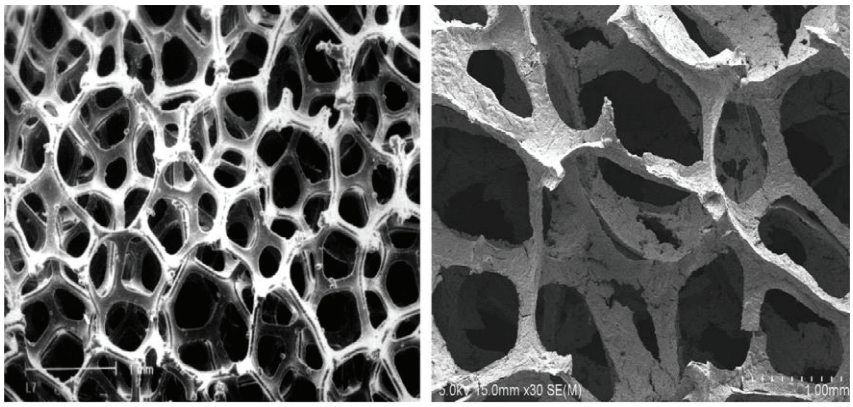

Figure 1.3. Three-dimensional reticulated foamed materials: (a) nickel foam; (b) iron foam (Source: Liu & Chen, First Edition 2014)

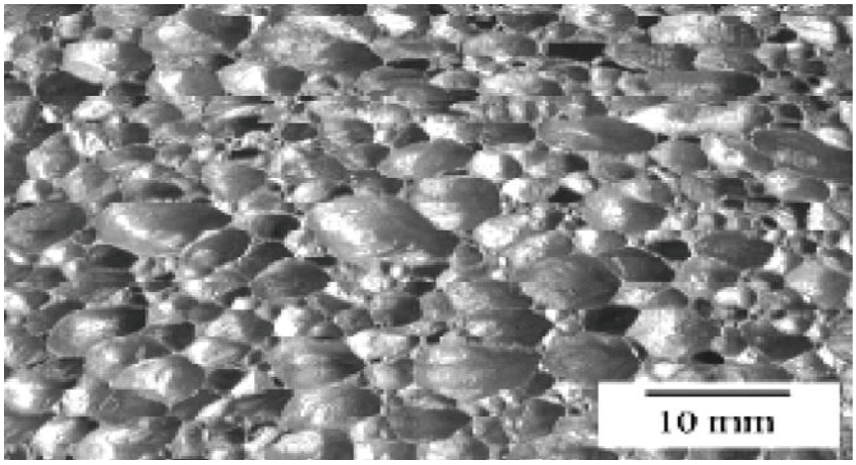

Figure 1.4. Bubblelike foamed materials (a closed-cell bubblelike foamed material of aluminum foam) (Source: Liu & Chen, First Edition 2014)

1.1. Motivation

The goals of present study are to

- investigate the mathematical model of bubble expansion in aqueous slurries composed of ceramic particles or powders.
- determine the expansions experimentally and
- combine the mathematical model with experimental results for bubble growth in pore formation.

1.2. Aerated Concrete

The aerated concrete (AC) is one of the types of light-weight concrete. Aerated concrete is also known as cellular concrete. The main advantage of using aerated concrete is its light-weight, which is economically feasible and functionally preferable for the design of supporting structures including foundation and walls of lower floors. AC provides a high degree of thermal insulation and considerable savings in material thanks to the porous structure. It is also fire resistant because air in the cells is responsible for high resistance to fire breakout, termite proof structure, and resistance to freezing. It has high sound absorption and acoustical insulation properties. Lastly, it is cost effective. Fly ash also saves considerable amount of investment on cement products. Hence it substantially diminishes the cost of construction.

There are quite many different applications of cellular light-weight concrete. It is utilized as thermal insulation in the form of bricks and blocks over flat roofs or non-loading walls. Bulk filling is intended for relatively low strength material used in old sewer pipes, wells, unused cellars and basements, storage tanks, tunnels and subways. Light-weight concrete is used in the production of heat-insulated light wall panel. It aims to prevent freezing in the bridge, and is also used for soil water drainage purposes.

Aerated concrete can be divided into two types depending on the method of production: foamed concrete (non-autoclaved aerated concrete (NAAC)) and autoclaved aerated concrete (AAC) (Hamad, 2014). Foamed concrete is produced by injecting preformed stable foam or adding a special air-entraining admixture known as a foaming agent into a base mix of cement paste or mortar (cement+water or cement+sand+water). AAC is produced by adding in a predetermined amount of aluminum powder and other additives into slurry of ground high silica sand, cement or lime and water (Figure 2.1.).

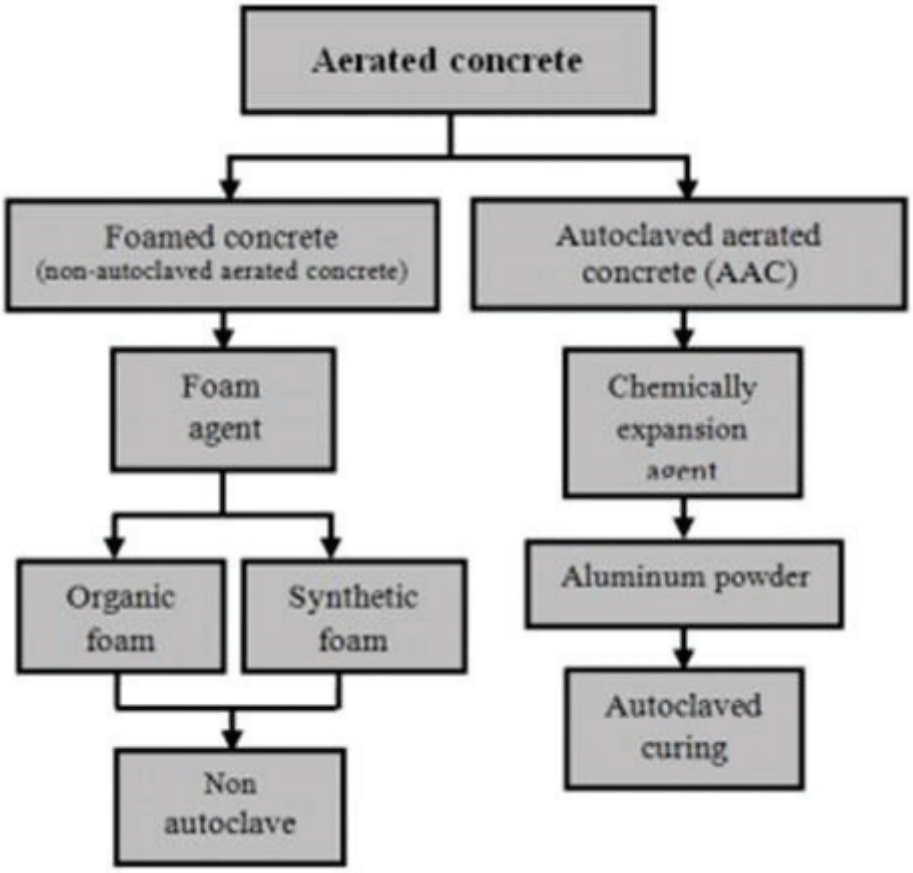

Figure 1.5. Classification of aerated light-weight concrete
(Source: Hamad, 2014)

The foam agent, (Hamad, 2014) which is the most essential influence on the foamed concrete, is used to obtain foamed concrete. When added into the mix water, foam agents produce discrete bubble cavities which become incorporated in the cement paste. Aluminum powder is used as a foaming agent in worldwide AAC production, and forms gas bubbles as a result of chemical reaction. Aluminum powder foaming agent is usually made from scrap foil in the form of microscopic flake-shaped aluminum particles.

Pore formation in cellular structures is accomplished by the chemical reactions that create gaseous reaction products. These reactions can take place at room or high temperature under solid or liquid state (Hamad, 2014). Hydrogen gas is created as a result of the reaction between aluminum and calcium hydroxide under room temperature. These reactions are given in section 2.2.1.

1.3. Foam Glass Materials

Foam glass is a light-weight material with the unique combination of following properties: rigid, compression-resistant, thermally insulating, freeze-tolerant, nonflammable, chemically inert and nontoxic, rodent and insect-resistant, bacteria-resistant and water and steam resistant. It allows quick construction, provides low transportation costs, and is easy to handle, cut and drill.

Foam glass is generally obtained by the use of a gas generating agent (foaming agent, mostly carbon or carbonaceous substances). The glass powder is initially mixed with a foaming agent in the powder form. The mixture of glass powder, foaming agent and other mineral agents is heated to a high temperature at which the mixture melts to form a viscous liquid and powder mixture. The viscous molten mixture then expands, and the foaming agent decomposes to generate a gaseous product. This event results in the formation of initially spherical small bubbles. As the gas pressure increases the foam cell structure transforms into polyhedral cells. After the cooling of glass they form the pores in foam glass. The process used here is called powder process, and currently all foam glass products are based on this method. The volume of gas bubbles or cells in a typical foam glass produced by powder process is 80%~95%. The bubble diameter ranges from 0.5 to 2 mm. The typical density is between 120 kg/m^3 and 160 kg/m^3 (Liyun, 1998).

The raw material of foam glass production today is the recycled waste glass or cullet. The cullet is obtained from a wide range of sources including used bottles, window glass, laminated glass, mercury lamps, industrial slag, fly ash, PC and TV-tubes, and batteries. The first foam glass was processed in 1930s by the direct introduction of gases into the molten glass (Scheffler & Colombo, 2005). This process consumed much more energy than the currently used powder process. Powder processing for foam glass production as outlined above is carried out at much lower temperatures, and can employ large quantities of powdered recycled glass. There is almost ten millions of waste glass every year, and a large percentage of it is in the form of crushed solids.

It is also noted that besides waste glass, other solid wastes increase in amount each year. One example is fly ash (Figure 1.6). Fly ash is produced with the combustion of coal in electric utility or industrial boilers. There are four basic types of coal-fired boilers: pulverized coal (PC), stoker-fired or traveling grate, cyclone, and

fluidized-bed combustion (FBC) boilers. The PC boiler is used for large electric generating units. The other boilers are used in industrial or cogeneration facilities. The physical and chemical characteristics of fly ash vary among combustion methods, coal source, and particle shape. In 2001, 62 million metric tons (68 million tons) of fly ash was produced whereas 20 million metric tons (22 million tons) or 32 percent of total production was used (Table 1.1). Remaining fly ash is used in the transportation industry. Today fly ash is used in a variety of engineering applications (Table 1.2). Typical uses are include portland cement concrete (PCC), soil and road base stabilization, flowable fills, grouts, structural fill and asphalt filler (Rafalowski, 2003). The fly ash in Portland cement increases the life of concrete roads and structures by improving concrete durability. The use in Portland cement also reduces the energy use and greenhouse gas effect. The other benefits include reduction of the landfills with fly ash, and conservation of the world's natural sources.

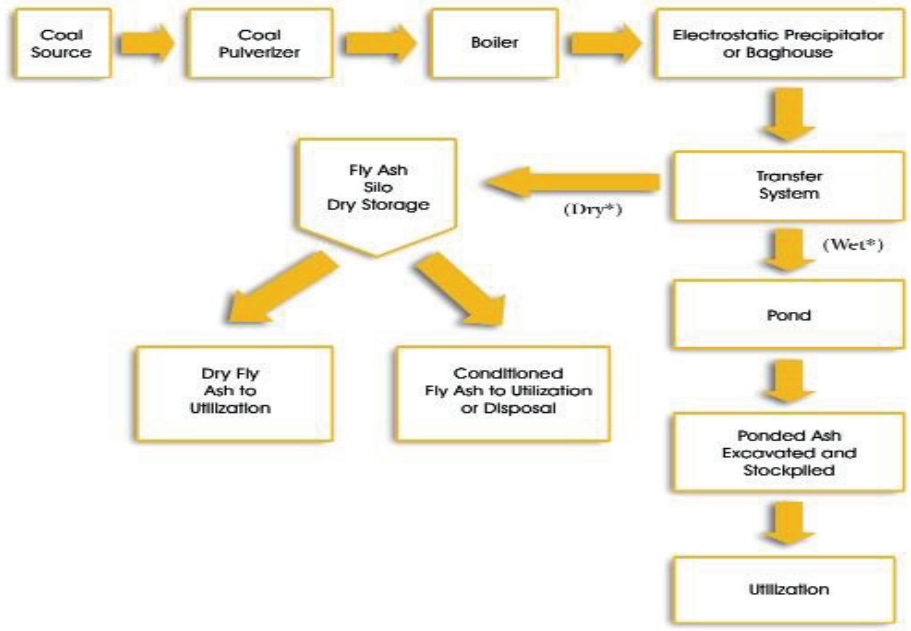

Figure 1.6. Conditioned fly ash to utilization or disposal
(Source: Rafalowski, 2003)

Table 1.1. Fly ash production and use
(Source: Rafalowski, 2003)

	Million Metric Tons	**Million Short Tons**	**Percent**
Produced	61.84	68.12	100.0
Used	19.98	22.00	32.3

Table 1.2. Fly ash uses
(Source: Rafalowski, 2003)

Materials	**Million Metric Tons**	**Million Short Tons**	**Percent**
Cement/Concrete	12.16	13.40	60.9
Flowable Fill	0.73	0.80	3.7
Structural Fills	2.91	3.21	14.6
Road Base/Sub-base	0.93	1.02	4.7
Soil Modification	0.67	0.74	3.4
Mineral Filler	0.10	0.11	0.5
Mining Applications	0.74	0.82	3.7
Waste Stabilization/Solidification	1.31	1.44	6.3
Agriculture	0.02	0.02	0.1
Miscellaneous/Other	0.41	0.45	2.1
Totals	19.98	22.00	100.00

Fly ash is finer than Portland cement and lime and usually silt-sized spherical particles typically ranging in size between 10 and 100 microns (Figure 2.3). These small glass spheres improve the fluidity and workability of fresh concrete. Fineness is one of the important properties contributing to the pozzolanic reactivity of fly ash.

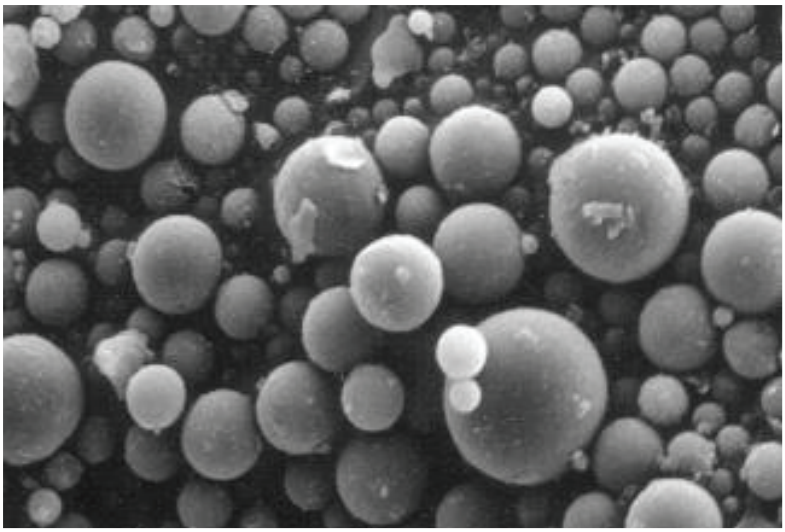

Figure 1.7. Fly ash particles at 2,000x magnification
(Source: Rafalowski ,2003)

The purpose of this thesis is to model the expansion behavior of aqueous slurries. Foamed or cellular material made using such method is known, especially in the concrete industry as explained earlier in this chapter. What appears to be lacking in the literature is the knowledge of pore formation and pore growth in inorganic particles based on aqueous slurry systems that result in the formation of cellular structures. The motivation of this study is to provide a scientific view in identifying and explaining the critical parameters that govern the pore growth and expansion of such slurry based systems.

The thesis is made up of three sections wherein the first section provides a general introductory overview on the topic. The second chapter describes the approach used in developing the mathematical model and the literature survey that has been used to support the model. Third chapter deals with the experimental approach of defining slurry expansion with the key systems and parameters used in developing the mathematical model. Fourth chapter provides a critique on the findings determined by modeling and experimental work.

CHAPTER 2

MATHEMATICAL MODELING

The chapter starts with providing a summary of literature that was used in developing the equations for the bubble growth phenomenon. This is followed by providing an explanation of how the model was built and the parameters used in developing the bubble growth equations. An application of the model based on empirical findings obtained from literature is given, showing the results on the ability of slurry systems to provide bubble growth and growth rate. The critical parameters that effect the bubble growth are provided.

2.1. Literature Survey on Mathematical Approaches on Pore Formation and Growth

One of the fundamental driving forces governing bubble growth depends on the pressure difference between the inside and outside pressure of a spherical cavity. Numerous studies ((Xiaoping, Zhifeng, Jiahua, & Hong, 2011), (Schwartzberg, Wu, Nussinovitch, & Mugerwa, 1995), (Wang, Ganjyal, Jones, Weller, & Hanna, 2005) and (Gent & Tompkins, 1969)) have been conducted based on this mechanism in order to define the models governing pore formation and growth. Diffusion is another important factor that defines the expansion of cavities. This factor is especially important in mechanisms involving high temperatures, as has been reported by Steiner (Steiner, 2006) in his study on the high temperature foaming of cellular structures using fly ash. This section will summarize some of the relevant mathematical modeling studies conducted in this area, which will later be used to derive the mathematical model presented in Section 3.2 of this study. It should be noted that studies related to high temperature expansion, and related models and mechanisms will not be discussed.

Wang et al. (Wang, Ganjyal, Jones, Weller, & Hanna, 2005) examined the modeling of bubble growth dynamics and non-isothermal expansion in starch-based foams during polymer extrusion. This model emphasizes three occurrences which are described sequentially as microbubble growth dynamics, couple bubble growth with extrude expansion, and macro transport phenomenon in the extrusion. The differential

equations involved in the model were solved by finite element schemes. Their study used the pressure difference mechanism for bubble formation and growth as the base mechanism to develop the models. This model uses the estimated radius, density and residual moisture of final extrude which were compared with experimental data. Lastly, this model was used to predict the profiles of downstream velocity, expansion ratio, moisture content, and temperature of extrude during expansion.

Schwartzberg et al. examined modeling deformation and flow during vapor-induced puffing. An equation describing bubble expansion in pseudo plastic fluids was modified to provide a differential equation describing vapor-induced pore expansion in foams formed in molten starch. The findings show that the flow yield stress (τ_0) at popping temperature acts to oppose whatever motion is taking place. They assumed that a yield pressure differential, ΔP_y, adheres to the below relationship developed by Yang and Yeh (Yang & Yeh, 1966) for bubble expansion in Bingham fluids:

$$\Delta P_y = \pm 3.464 \tau_0 \left[\frac{1}{3} + \ln\left(\frac{L}{R}\right)\right] \tag{2.1}$$

Where τ_0 is the flow yield stress and R is the radius of the bubble, Yang et al. (Yang & Yeh, 1966) theoretically investigated bubble dynamics in purely viscous fluids. They analyzed the growth or collapse of a spherical bubble in an incompressible, viscous fluid. Their results show the variations in the bubble size and its growth or collapse rate, the fluid pressure and the rate of energy dissipation. Their analysis and approach may be applied to Newtonian and non- Newtonian fluids. A comparison is given for the collapse of bubble in several viscous fluids. According to this theoretical study (Yang & Yeh, 1966), equation for bubble motion is given below;

$$\ddot{R}^0\left[-\frac{(R^0)^2}{r_0^2} + R^0\right] + \left(\dot{R}^0\right)^2\left[-\frac{2R^0}{r_0^0} + \frac{(R^0)^4}{2(R_0^0)^4} + \frac{3}{2}\right]$$

$$= p_g^0 - p_l^0\left(r_0^0\right) - \frac{2\sigma^0}{R^0} - \left(\eta^0 + \mu_g^0\right)\frac{\dot{R}^0}{R^0} \pm 2\sqrt{3}\,\frac{\tau_0}{\Delta p}\left[\ln\left(\frac{r_0^0}{R^0}\right) + 1/3\right] \tag{2.2}$$

In this theoretical study, equation (2.2) contains the parameters that are given below,

R = Bubble radius

R_0 = Initial bubble radius, r_0 = Refence radius

$$\dot{R} = \frac{dR}{dt} \tag{2.3}$$

$$\ddot{R} = \frac{d^2R}{dt^2} \tag{2.4}$$

$$R^0 = \frac{R}{R_0} \tag{2.5}$$

$$\dot{R^0} = \dot{R}\left(\frac{\rho_l}{\Delta P}\right)^{1/2} \tag{2.6}$$

$$\ddot{R^0} = \ddot{R}R_0\,{}^{\rho_l}/_{\Delta P} \tag{2.7}$$

$$r_0{}^0 = \frac{r_0}{R_0} \tag{2.8}$$

$$p_g^0 = \frac{p_g(R) - p_{g0}}{\Delta p} \tag{2.9}$$

$$p_l^0 = \frac{p_{l0}(r) - p_{g0}}{\Delta p} \tag{2.10}$$

Pressure is, $p_g(R)$, of gas at bubble wall, p_{g0} , of gas inside at zero time, $p_{l0}(r)$, of liquid at zero time.

η = Parameter of Bingham model

$$\eta^0 = \left(\frac{\eta}{R_0}\right)\left(\frac{1}{\rho_l \Delta p}\right)^{1/2} \tag{2.11}$$

$$\mu_g^0 = \left(\frac{\mu_g}{R_0}\right)\left(\frac{1}{\rho_l \Delta p}\right)^{1/2} \tag{2.12}$$

The below relation from equation (2.2) provides the equation for Bingham plastic model:

$$P_y = \pm 2\sqrt{3}\,\frac{\tau_0}{\Delta p}\left[\ln\left(\frac{r_0}{R}\right) + {}^1/_3\right] \tag{2.13}$$

P_y =Yield stress pressure

τ_0 =Yield stress of Bingham model

r_0 =Refence radius

R= Bubble radius

Δp= Pressure difference, P_∞-P_{g0}

P_∞=Pressure of liquid at infinity or system pressure

P_{g0}= Pressure of gas inside at zero time

The study (Yang & Yeh, 1966) provides another equation for bubble motion which is;

$$R^0\ddot{R}^0+\frac{3}{2}\left(\dot{R}^0\right)^2=p_g^0-p_\infty^0-\frac{2\sigma^0}{R^0}-4\left(\mu_l^0+\mu_g^0\right)\frac{\dot{R}^0}{R^0} \quad (2.14)$$

This equation's right side describes Newtonian flow which is given as:

$$P_y=4\left(\mu_l^0+\mu_g^0\right)\frac{\dot{R}^0}{R^0} \quad (2.15)$$

$$\mu^0=\left(\frac{\mu}{R_0}\right)\left(1/\rho_l\,\Delta p\right)^{1/2} \quad (2.16)$$

Where μ is viscosity, μ_l is the viscosity of liquid and μ_g is viscosity of gas.

$$P_y=-\frac{4}{R}\mu_l\frac{dR}{dt} \quad (2.17)$$

Gent and Tompkins (Gent & Tompkins, 1969) examined the nucleation and growth of gas bubbles in elastomers. They found a critical condition for bubble formation in most cases. The gas super saturation pressure must exceed $5G/2$, where G is the shear modulus of the elastomers. They showed that the kinetics of bubble growth in good accord with a simple diffusion- controlled growth relation for a variety of gases, elastomers, temperatures, and pressures. Inflation of an initially present small spherical hole is assumed to be resisted by elastic forces and surface tension in the rubber. The relation between the pressure P inside the hole and the radius R is then given by the following equation:

$$P=G\left[\frac{5}{2}-2\left(\frac{R_0}{R}\right)-\frac{1}{2}\left(\frac{R_0}{R}\right)^4+\left(\frac{2\sigma}{GR}\right)\right] \quad (2.18)$$

Where G is the shear modulus of the rubber, R_0 is the initial bubble radius, R is the bubble radius and σ is the surface tension of the rubber.

Fan et al. (Xiaoping, Zhifeng, Jiahua, & Hong, 2011) investigated nucleation and growth of bubbles in elastomers. In their approach, an experimental study is used to describe the formation and growth of gas bubbles in cross-linked elastomers. They provide the below equation that estimates how pressure, P, varies as bubble radius, R, increases when a bubble expands in an infinite elastic domain, i.e. $P_e = 0$ when expansion starts, approaches a maximum of 5E/2 as expansion proceeds,

$$\frac{P_e}{E} = \frac{5}{2} - \frac{2R_0}{R} - \frac{1}{2}\left(\frac{R_0}{R}\right)^4 \left(\frac{L^3 - R^3}{L^3 + 2R^3}\right) \tag{2.19}$$

R_0= Initial value of R (m)

L= Domain radius (m)

R= Pore radius (m)

E= Shear modulus (N/m2)

2.2. Model Parameters and Assumptions

It is assumed that the bubble expansion rate depends on the pressure difference, ΔP, between the inside and outside pressure. This relation is written as follows;

$$\Delta P = P_i - (P_s + P_t + P_y + P_e + P_h) \tag{2.20}$$

Where;

P_i= The pressure inside of a bubble

P_s= Atmospheric pressure

P_t= Pressure due to surface tension

P_e= Pressure due to elastic stress

P_y= Pressure due to yield stress

P_h= Hydrostatic pressure

The dependence of ΔP to the 6 parameters identified above is explained in sections 2.2.1. to 2.2.6. A model is, therefore, formed that ultimately aims to relate ΔP to the change in pore size, in the form of radium, R. This overall model equation is summarized in section 2.2.7. of this chapter.

In order to apply the model, the equations have been assumed based on spherical coordinates. These assumptions are given below;

1. Bubbles are not compressible and the solid-liquid suspension density is homogeneous and constant within time ($\frac{\partial \rho}{\partial t}=0$ and $\nabla\rho=0$)
2. The solid-liquid suspension acts either as a Newtonian or a Bingham Plastic Fluid.
3. The bubble is spherical, which suggests that all expressions for the directions perpendicular to radial one are eliminated ($\upsilon_\theta=\upsilon_\phi=0$ and $\frac{\partial}{\partial\theta}=\frac{\partial}{\partial\phi}=0$)
4. Foaming gases, formed as a result of solid and/or liquid state reactions, determine bubble formation and growth. Foaming gases are assumed to be formed by the generation of hydrogen gas, which is based on the room temperature and atmospheric pressure reaction between Al metal and $Ca(OH)_2$.

These model assumptions give us some approaches to explain occurrence and growth of bubbles within these conditions. First assumption is the equation of continuity which exhibits;

$$\frac{\partial \rho}{\partial t}=-(\nabla.\rho\upsilon) \tag{2.21}$$

Where ρ is the fluid density, t is the time and υ is the mass average velocity vector, the first assumption ($\nabla\rho = 0$) suggests the following;

$$(\nabla.\upsilon)=0 \tag{2.22}$$

In the third assumption (Spherical symmetry);

$$(\nabla.\upsilon)=\frac{1}{r^2}\frac{\partial}{\partial r}(r^2\upsilon_r)=0 \tag{2.23}$$

Where r is the radial coordinate in spherical coordinates and υ_r is the mass average velocity of the fluid in the r direction, integration of this equation is as below:

$$r^2\upsilon_r = \text{constant} = R_1^2\upsilon_{R1} \Leftrightarrow \upsilon_r=\frac{R_1^2}{r^2}\upsilon_{R1} \tag{2.24}$$

R_1 is the inner radius of the bubble, R_2 is the outer radius of the bubble (which is infinity) and υ_{R1} is the growth rate of the bubble radius R_1, $\upsilon_{R1}=\frac{dR_1}{dt}=\dot{R}$. This condition allows us to relate ΔP to the changes in pore radius as a function of time.

2.2.1. The Pressure Inside of a Bubble

The pressure inside of a bubble is assumed to be formed by the generation of hydrogen gas occurrence rate, which is based on the room temperature and atmospheric pressure reaction between aluminum metal and calcium hydroxide.

According to researchers, scientists studied the mechanism of aluminum powder corrosion in calcium hydroxide solutions which was examined via various analyses of residues after its hydrolysis reaction and pH change of the solutions to control the release of hydrogen gas. It was unveiled that the reaction with release of hydrogen gas was involved in katoite formation and hydration of aluminum. The katoite formation, which is driven by the reaction among calcium ion, aluminum hydroxide anion ($Al\ (OH)_4-$), and water molecules at the first step, is important for the promotion of aluminum corrosion and moderate release of hydrogen gas. (Kanehira, et al., 2013)
These reactions are given as follows:

$$Al_2O_3+H_2O\rightleftarrows 2AlOH \quad (2.25)$$

$$AlOH+H_2O\rightleftarrows Al(OH_3) \quad (2.26)$$

$$Al(OH_3)+OH\rightleftarrows Al(OH)_4^- \quad (2.27)$$

$$3Ca^{2+}+2Al(OH_4)+8H_2O\rightleftarrows Ca_3Al_2(OH)_{12}+6H_2 \quad (2.28)$$

According to equation (2.28), bubble expansion phenomenon consists of 3 calcium ions that react with 2 aluminum molecules. After that, 6 moles of hydrogen gases are released. This reaction kinetics aims to release hydrogen gases. Al_2O_3, which is different from bulk, is shown in equation (2.25). The thin passive layer reacts with water and disruption of Al – O –Al bonds. It occurs by the way of hydrolysis reaction to form theAl – OH species. Al – O –Al bonds are broken to form two Al – OH for each water molecule consumed in the hydrolysis reaction in equation (2.25). The water molecule tends to attack the aluminum. Then, extensive hydration propagates the formation of boehmite, γ-AlOOH or aluminum hydroxide, $Al(OH)_3$, which are

thermodynamically more stable than Al_2O_3. The amorphous $Al(OH)_3$ tends to dissolve into $Al(OH)_4^-$ion equation (2.27). Ca_2^+,$Al(OH)_4^-$ ions and water molecule consist the following reaction which takes part in equation (2.28). These reactions are shown in Figure 2.1 which contains four stages. All stages explain the release of hydrogen gases via equation (2.25) to (2.28).

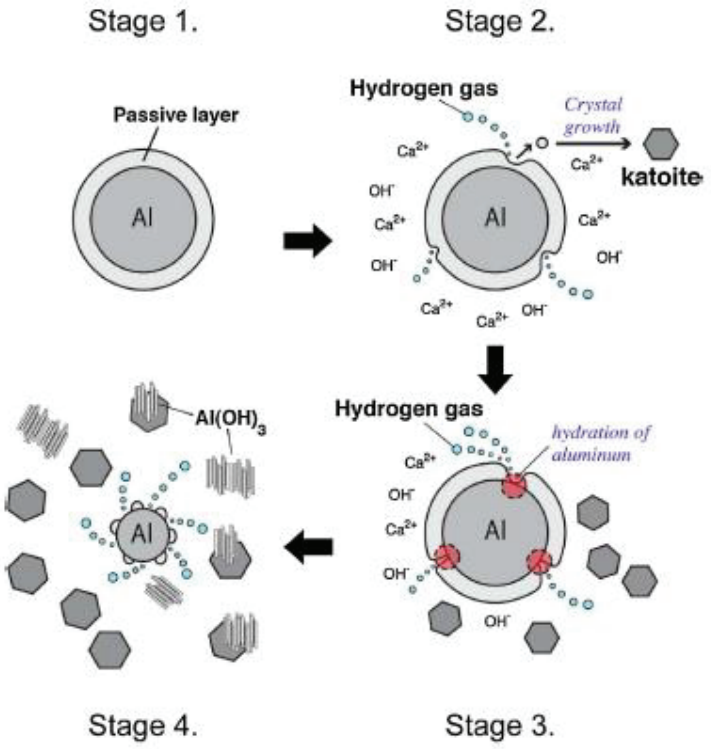

Figure 2.1. Model of the aluminum corrosion in $Ca(OH)_2$ solution. The corrosion reactions progress from the stage 1 to 4. (Source: Kanehira, et all., 2013)

Hydration of aluminum powder mainly includes the release of hydrogen gas following the equations (2.25) to (2.27) after the surface oxide dissolves into the solution and localized breakdown occurs as shown in stage 3 (small circle). As these reactions proceed, the size of aluminum decreases as shown in stage 4. Eventually, aluminum dissolves into the solutions completely, and release of hydrogen stops.

The study reveals the amount and rate of hydrogen gas release, which is provided in Figure 2.2. The results show that using different aluminum to calcium hydroxide ratios will have a significant influence on the release of hydrogen gases.

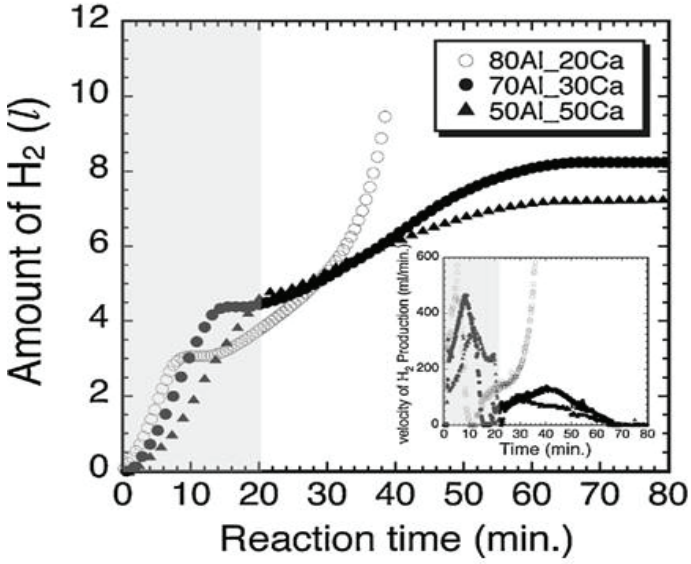

Figure 2.2. Volume change in hydrogen gas
(Source: Kanehira, et al., 2013)

According to ideal gas equation;

$$PV=nRT \tag{2.29}$$

n=6 mol V=4.5 l.

R=0.0082 $\frac{\text{l. atm}}{\text{mol.K}}$ T=25 ℃=298 K

$$P_i=3.25 \text{ atm} \tag{2.30}$$

2.2.2. Atmospheric Pressure

Atmospheric pressure is the force per unit area exerted on a surface by the weight of air above that surface in the atmosphere of Earth. In simple terms, atmospheric pressure is also the same as air pressure. Atmospheric pressure has been taken as 1 atm (101,325 Pa) in the calculations for this model.

2.2.3. Pressure Due to Surface Tension

Surface tension is the elastic tendency of liquids which makes them occupy the least surface area possible. Laplace equation has been used to represent the pressure due to surface tension (Xiaoping, Zhifeng, Jiahua, & Hong, 2011):

$$P_t = \frac{2\sigma}{R} \tag{2.31}$$

Where, P_t is the pressure due to surface tension, σ is the surface tension and R is the radius of the pore. Surface tension value of 0.7197 N/m has been used in reference to the glass-water surface energy from literature (Vargaftik, Volkov, & Voljak, 1983).

2.2.4. Pressure Due to Yield Stress

Yield pressure equation for Bingham plastic fluids was given in equation (2.13) and for Newtonian fluids in equation (2.17). Δp in the equation has been assumed to have a value of 3.25 atm, where $P_\infty = P_i$=3.25 atm and $P_{g0} = 0$.

2.2.5. Pressure Due to Elastic Stress

Equations (2.18) and (2.19) describe the elastic stress pressure. Equation (2.19) is used for the modeling of this study since the domain radius, L, is much greater than the pore radius R (Gent & Tompkins, 1969).

2.2.6. Hydrostatic Pressure

Hydrostatic pressure in a liquid can be determined using the following equation:

$$P = \rho g h \tag{2.32}$$

Where ρ is the density of liquid, g is the gravitational constant and h is the height of fluid column, or in the fluid at which the pressure is measured. The hydrostatic properties of a liquid are not constant, and the main factors influencing it are the density of the liquid and the local gravity. Both of these quantities need to be known in order to determine the hydrostatic pressure of a specific liquid. Liquid density, ρ=1,000 $kg/m^3$and g=9.81 m/s^2 values have been used in the modeling of this study.

2.2.7. Overall Pressure Difference Equation

Based on the equations and assumptions derived in sections 2.2.1. to 2.2.6., the following overall pressure differential equation is developed.

For Newtonian liquids:

$$\Delta P = [3.25\ \text{atm}]\text{-}\left[(1\ \text{atm}) + \frac{2\sigma}{R} + \left(-4\frac{\mu_l}{R}\dot{R}\right) + E\left[\frac{5}{2} - \frac{2R_0}{R} - \frac{1}{2}\left(\frac{R_0}{R}\right)^4\right] + \rho gh\right] \quad (2.33)$$

For Non-Newtonian, Bingham plastic liquids:

$$\Delta P = [3.25\ \text{atm}]\text{-}\left[(1\ \text{atm}) + \frac{2\sigma}{R} + \left(\pm 2\sqrt{3}\frac{\tau_0}{\Delta p}\left[\ln\left(\frac{r_0}{R}\right) + {}^1\!/_3\right]\right) + E\left(\frac{5}{2} - \frac{2R_0}{R} - \frac{1}{2}\left(\frac{R_0}{R}\right)^4\right) + \rho gh\right] \quad (2.34)$$

The definitions of each term have been given in the prior sections.

2.3. Mathematical Modeling System

Mathematical model system uses the pressure difference between the inside and outside of a spherical bubble as the driving force for defining growth. As is discussed in section 2.2.1., the study conducted by Kanehira at al. (Kanehira, et al., 2013) shows the mechanism of aluminum powder corrosion in calcium hydroxide solutions, which was examined via various analyses of residues after its hydrolysis reaction and pH change of the solutions to control the release of hydrogen gas. Figure 2.1 shows the effects of different aluminum and calcium ratios on the release amount and release rate of hydrogen. This empirical examination of three different ratios has been taken as case studies to solve the model equation developed in this study in section 2.2.7. Accordingly, there are three different ratios: 50% Al - 50% $Ca(OH)_2$, 70% Al - 30% $Ca(OH)_2$ and 80% Al – 20% $Ca(OH)_2$ that have been used in this study to determine the change in pressure within a cavity.

The curves in Figure 2.2 illustrate that they are formed of two parts: first part shows a linear rate while second part is parabolic. A start and an end point have been identified for these two parts of the curves and a corresponding equation have been determined, as explained in further detail in Appendix A. Accordingly, the reaction involving 50%Al – 50% $Ca(OH)_2$ (50/50) is associated with a linear and a parabolic equation as given below:

$$R = \left(\frac{27}{160\pi}t\right)^{1/3} \quad (2.35)$$

$$R = (0.005(t-14)^2 + 1.07)^{1/3} \quad (2.36)$$

The remainder of the linear and parabolic parts of the equations for Al/Ca ratios of 70/30 and 80/20, together with 50/50 ratio shown above are given in Table 3.1.

Table 2.1. Radius – Time equation

Al/Ca(OH)$_2$ Ratio	**Linear**	**Parabolic**	**Equation No.**
50/50	$R = \left(\frac{27}{160\pi}t\right)^{1/3}$	$R = (0.005(t-14)^2 + 1.07)^{1/3}$	(2.35),(2.36)
70/30	$R = \left(\frac{27}{112\pi}t\right)^{1/3}$	$R = (0.004(t-14)^2 + 1.07)^{1/3}$	(2.37),(2.38)
80/20	$R = \left(\frac{9}{32\pi}t\right)^{1/3}$	$R = (0.001(t-8)^2 + 0.71)^{1/3}$	(2.39),(2.40)

It has been discussed in section 2.2.1. that the bubble expansion rate depends on the pressure difference between the inside and outside pressure which was shown to depend on six different parameters. These parameters are ultimately considered to have a direct effect on bubble expansion. This theoretical approach will be used to find possible correlations between the empirical hydrogen gas release equations developed from three different Al/Ca(OH)$_2$ ratios. A relation is found showing the changes in pressure as a function of time, and therefore pore radius will be calculated using these equations. This relationship was calculated using Wolfram Mathematica software.

The changes in ΔP as a function of change in bubble radius for the linear and parabolic parts of the equations have been plotted in Figures 2.3 to 2.5 for the 50/50, 70/30 and 80/20 Al/Ca(OH)$_2$ ratio reaction conditions.

First of all, 50/50 ratio is shown below,

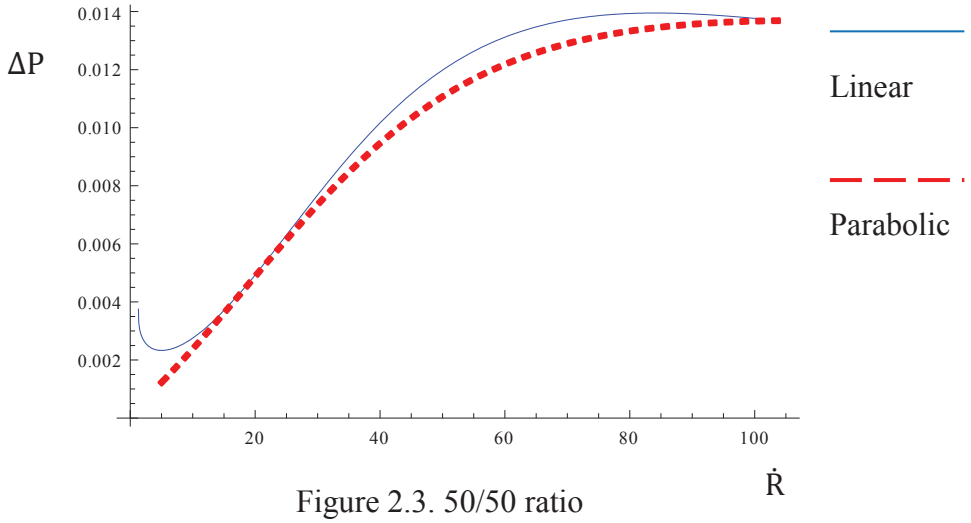

Figure 2.3. 50/50 ratio

Bubble expansion ratio in 50/50 provides a linear decrease of bubble expansion from the baseline to 5 minutes, and this linear decrease can be called the bubble's nucleation field which is an estimation of foaming agent. 5 minutes later, nucleation energy is surpassed which suggests that bubble expansion phenomenon has a parabolic augmentation.

Second step is 70/30 ratio which is given as follows,

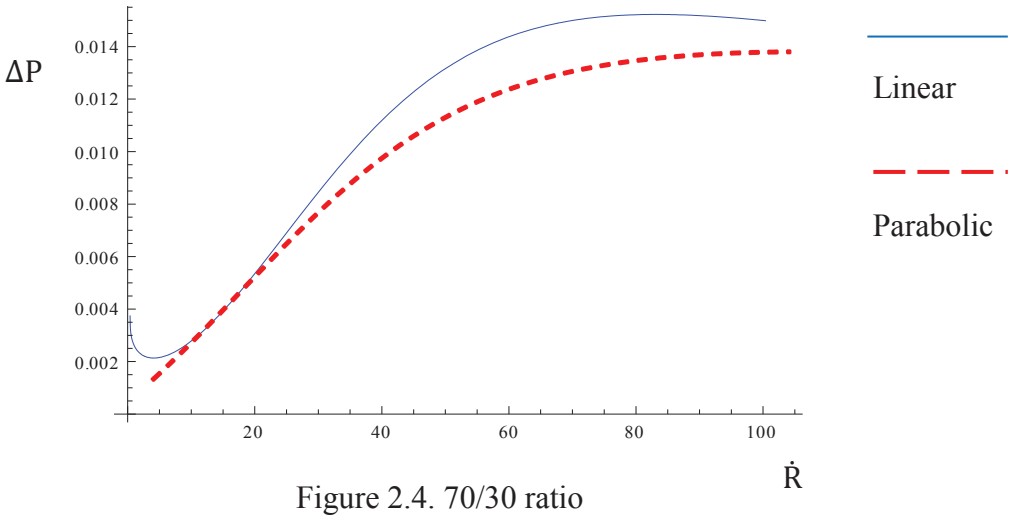

Figure 2.4. 70/30 ratio

Linear decrease and parabolic augmentation of bubble expansion have the same form between 70/30 and 50/50. It has a linear decrease of bubble expansion from the baseline to 3 minutes, and this linear decrease can be called bubble's nucleation field. Later, it increases until 70 minutes, and then remains stable.

Third step is 80/20 ratio which has a different linear decrease and parabolic augmentation as compared to 70/30 and 50/50. Aluminum ratio is higher than the others and, has a different linear decrease that takes part as follows,

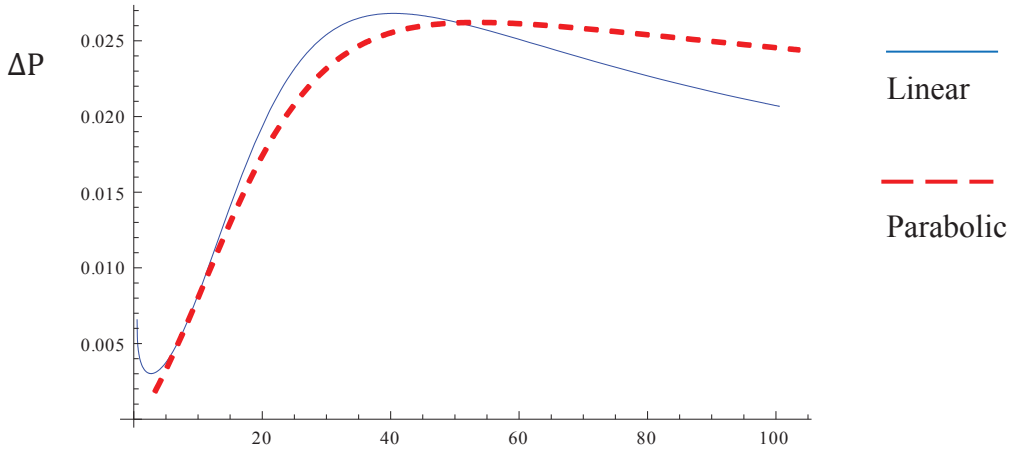

Figure 2.5. 80/20 ratio $\dot{R}$

In 80/20 ratio, 80% aluminum reacts with 20% calcium hydroxide, which provides a linear decrease of bubble expansion from the baseline to 2 minutes. Then it expands rapidly.

Bubble expansions for pore formation's mathematical models have been plotted in figure 2.3 to 2.5. Blue lines are linear plots, and red lines are parabolic plots. According to the overall pressure differential equation for Newtonian liquids equation (2.23), pressure difference is associated with derivation of bubble radius. In the figure 2.3 to 2.5, pressure difference includes a random unit. In this study, derivation of bubble radius compares with experimental studies. When calcium hydroxide ratio decreases, baseline bubble expansion ratio decreases. This explanation is examined in section 2.2.1, and discussed in chapter 4, which can also be called the bubble's nucleation field. In this field, bubble does not have enough energy. When it has enough energy, it expands rapidly, which is called parabolic line.

CHAPTER 3

EXPERIMENTAL STUDIES

The experimental part of this study aims to find possible correlations with the mathematical modeling part defined in Chapter 3. This chapter includes the explanation of the experimental procedures used in preparing the aqueous slurries, and the measurement of their expansion behavior. A presentation of the results obtained from these measurements is provided.

3.1. Materials and Methods

Slurries were prepared using crushed glass powder (Potters Industries, LLC, USA), calcium hydroxide powder (Akg Gazbeton, LLC, Turkey), carboxymethyl cellulose (Sigma Aldrich, LLC, USA), aluminum paste (Akg Gazbeton, LLC, Turkey), Triton x-100 (Sigma Aldrich, LLC, USA) and deionized (DI) water. All the slurries used in this study were based on 51.6 weight % solids and the remainder being DI water. Crushed glass was screened to fit in a size range between 45 to 56 micrometers using sieves (Fritsch, LLC, Germany).

3.1.1. Slurry Preparation

Table 3.1 provides the weights of all the ingredients used in preparing the slurry. The weights of the expansion agents (Al and $Ca(OH)_2$) were based on the study conducted by Kanehira et al. (Kanehira, et al., 2013), the details and mechanisms of which have been explained in prior sections. In the preparation of slurry, aluminum was the last ingredient added so as to monitor and measure the expansion behavior. Carboxymethyl cellulose (CMC) was used to promote a steric stabilization and to provide a green strength to the dried material after expansion. CMC was added and dissolved in DI water before any other solid particle was introduced. Glass powder, and calcium hydroxide powder were added and mixed manually for a few minutes. The aluminum powder, which was supplied as a mixture in an organic formulated paste form, was mixed in a separate cup with 1 g DI water and Triton x-100. Triton x-100 is a surfactant which helps to disperse the aluminum particles. The aluminum mix was then

added to the remainder of the water solids mixture and mixed manually. Expansion was monitored, as explained in the following section.

Table 3.1. Amounts of ingredients used in the preparation of slurries.

Materials	**Al/Ca(OH)$_2$ Ratio**		
	50/50	**70/30**	**80/20**
Glass Powder	20.0 g	20.0 g	20.0 g
Aluminum	0.374 g	0.524 g	0.60 g
Calcium Hydroxide	0.374 g	0.224 g	0.150 g
Carboxymethyl cellulose (CMC)	0.60 g	1.00 g	1.00 g
Triton x-100	0.30 g	0.30 g	0.30 g
Deionized Water	20.29 g	20.29 g	20.29 g

3.1.2. Expansion Measurements

The expansion of slurries after preparation was monitored and measured using a laser-based data logging system. The slurries were prepared inside a Teflon base and a Teflon tube in order to minimize friction. The resolution of the laser is ±1mm. The experimental set-up used in this measurement is shown in Figure 3.1. The expansion was monitored once aluminum was introduced into the slurry, which is considered the starting point of reaction. Teflon tube was placed in the first and second expansion of slurry. The third expansion of the slurry was also monitored using a camera where the slurry was placed in a clear plexiglass tube. The plexiglass tube was used as-is with no oil or surface release agent used during the expansion process and, is shown in Figure 3.2.

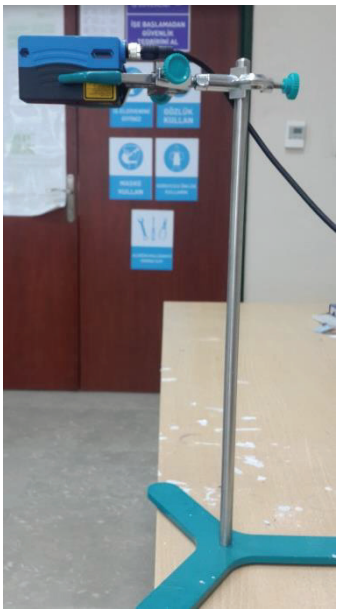

Figure 3.1. Laser distance sensor

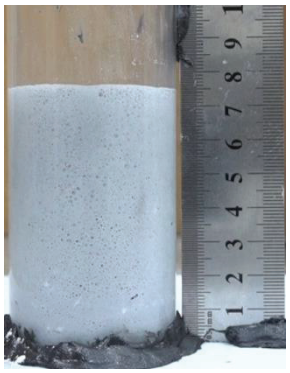

Figure 3.2. Bubble expansion

3.2. Presentation of Experimental Results

Bubble growth phenomenon has been presented theoretically in the prior section. In the view of theoretical study, experimental results are given. Experimental study consists of three different aluminum and calcium hydroxide ratios which are 50/50, 70/30, and 80/20. These experimental studies, which include a teflon tube, are repeated twice, and their relations are given in Figure 3.3 to 3.5. Then, these experimental studies are combined in Figure 3.6where, firstly 50/50, 70/30 and 80/20

ratios increase linearly. Secondly these ratios are stable and lastly, these ratios decrease slowly. According to figure 3.3 to 3.5, bubble growth phenomenon are plotted within second graphs in the all aluminum and calcium hydroxide ratios and given figure 3.6. In the third expansion, bubble expansion phenomenon is recorded with a camera, and these images are shown in Appendix B. The slurry placed in a clear plexiglass tube is shown Figure 3.2.

Accordingly, experimental study of bubble expansion phenomenon depends on the pressure difference in the slurry. Firstly, 50/50 ratio is described below;

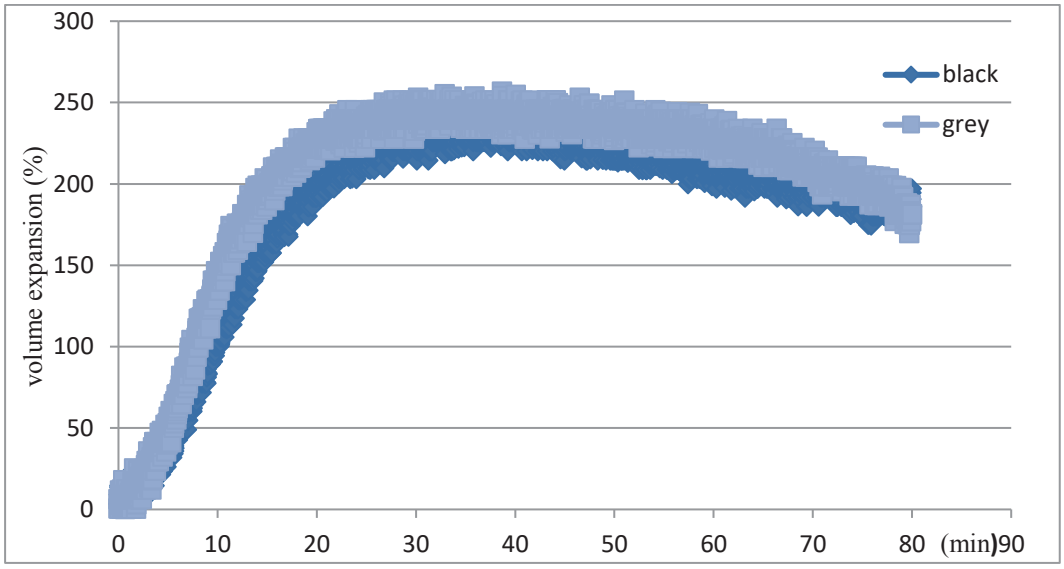

Figure 3.3. 50/50 ratio volume expansion percentage - time

Where, volume expansion percentage versus time graph is plotted. There are two experimental graphs in the 50/50 ratios. Black and grey plots are nearly the same. They increase to 25 minutes linearly, and are stable between 25 and 40 minutes. Then they decrease slowly.

Secondly, 70/30 ratio is described in Figure3.4. Where, there are two experimental graphs in the 70/30 ratios. Black and grey plots are nearly the same. They increase to 10 minutes linearly, are stable between 10 and 25 minutes, and decrease until 80 minutes.

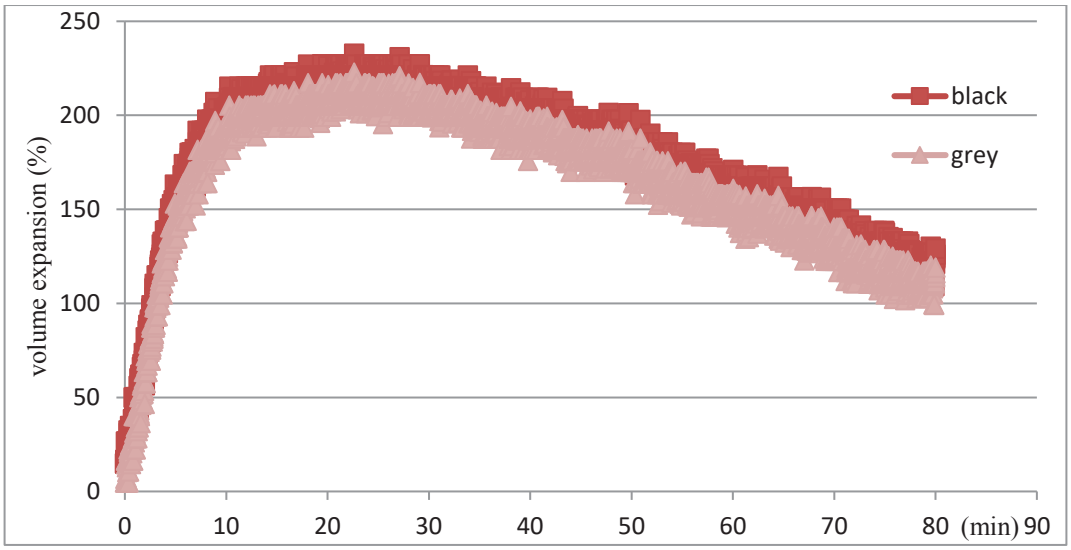

Figure 3.4. 70/30 ratio volume expansion percentage - time

Thirdly, 80/20 ratio is described below;

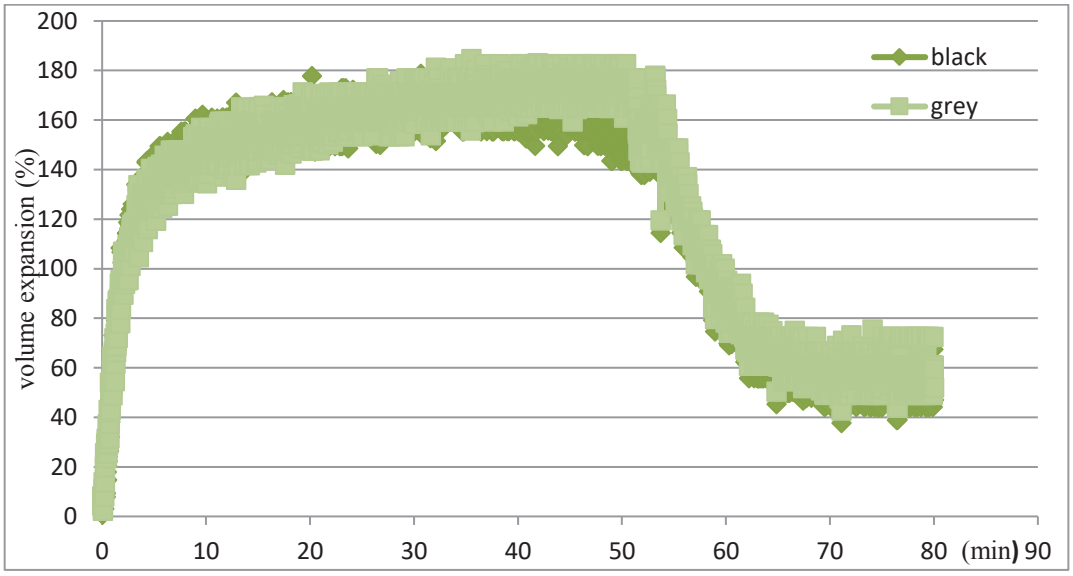

Figure 3.5. 80/20 ratio volume expansion percentage - time

Where, there are two experimental graphs in the 80/20 ratios. Black and grey graph have the same linearity until 50 minutes. They increase sharply until 10 minutes, are stable but after 55 minutes, and then decrease slowly.

Bubble growth for pore formation is combined for 50/50, 70/30, 80/20 ratios which are plotted below,

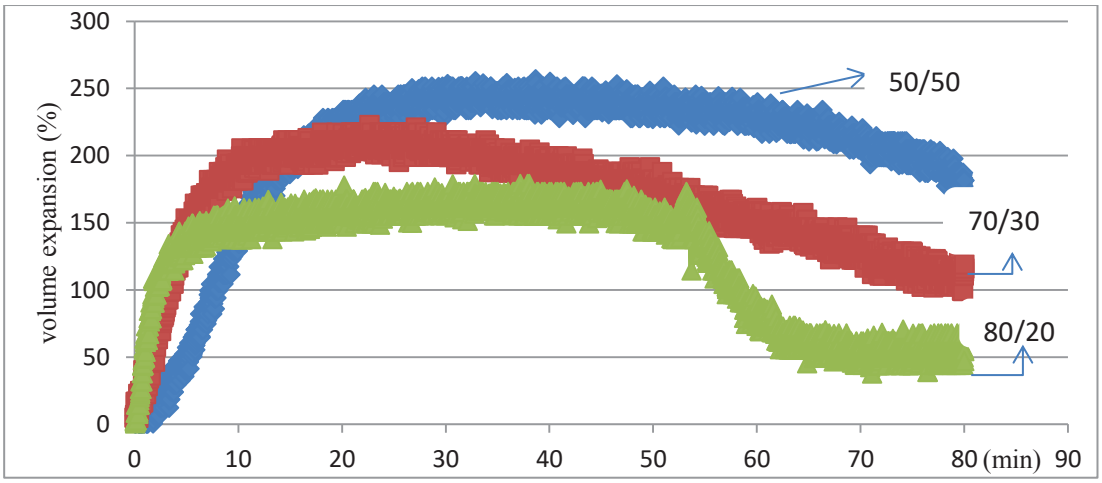

Figure 3.6. 50/50, 70/30, 80/20 volume expansion percentage - time

Where, there are three experimental graphs in the 50/50, 70/30 and 80/20 ratios. First graph is 50/50, second graph is 70/30, and third graph is 80/20. Experimental study shows that the maximum volume expansion percentages are 250%, 200% and 160% for 50/50, 70/30 and 80/20, respectively. All graphs have the same morphology. Firstly, they increase linearly. Secondly, they are stable. Lastly, they decrease slowly.

The third expansion of the slurry is monitored using a camera which is shown in Appendix B. The slurry placed in a clear plexiglass tube is shown in Figure 3.2. Third expansion is given in Figure 3.7 which has three experimental graphs in the 50/50, 70/30 and 80/20 ratios. First graph is 50/50, second graph is 70/30, and third graph is 80/20 which are given below,

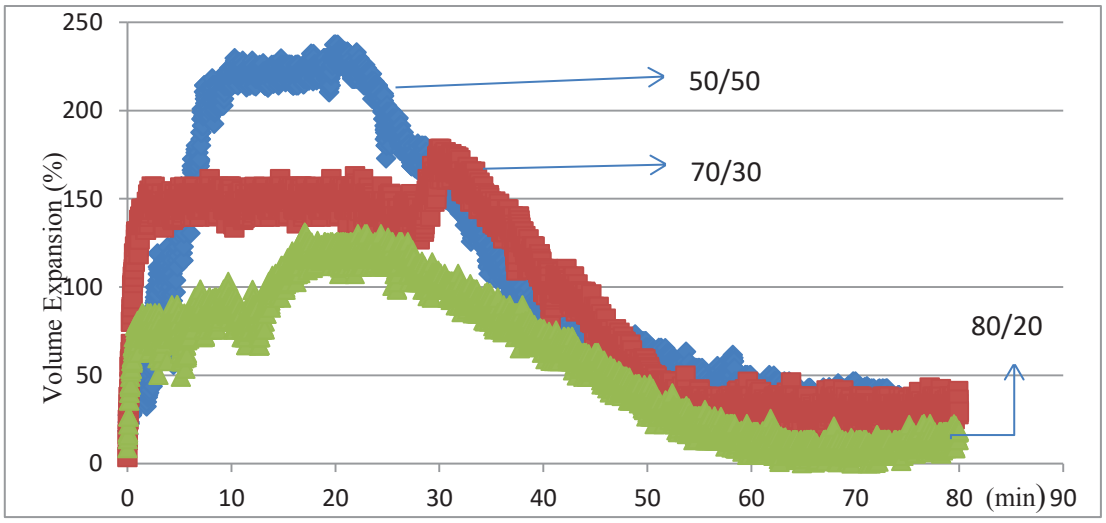

Figure 3.7. 50/50, 70/30, 80/20 volume expansion percentage – time in the plexiglass

Experimental study shows that the maximum volume expansion percentages are 230%, 180% and 120% for 50/50, 70/30 and 80/20, respectively. All graphs have the same morphology. Firstly, they increase linearly. Secondly, they are stable. Lastly, they decrease slowly. Bubble expansion phenomenon is discussed in chapter 4.

CHAPTER 4

DISCUSSION OF RESULTS AND FINDING

Bubble expansion phenomenon is examined in 2 sections which are chapter 2 and 3. Mathematical modeling and experimental studies of bubble expansion phenomenon are described in this study. In mathematical modeling, there is an application of the model based on empirical findings obtained from literature, providing the bubble growth and growth rate. The critical parameters that affect bubble growth are enabled. Bubble expansion phenomenon has a reaction between aluminum and calcium hydroxide, and is used in this study theoretically and experimentally. This reaction is examined using the empirical findings (Kanehira, et al., 2013). The empirical finding is the volume change of hydrogen gas at about 50/50, 70/30, 80/20 obtained from gas flow meter as shown in Figure 2.2. Where, vertical position is the amount of hydrogen gases, and horizontal position is the time interval. According to overall pressure differential equation for Newtonian liquids equation (2.23), pressure difference is associated with the derivation of bubble radius. Mathematical model is developed from empirical findings, which is shown in Figure 2.3 to 2.5. These figures vertical positions refer to the pressure difference between inside and outside pressure, and their horizontal positions point out the derivation of bubble radius. Vertical positions are random units because of empirical findings. Firstly, graphs generally have linearity and secondly, they have parabolic system. In the 50/50 ratio, it has a linear decrease of bubble expansion from the baseline to 5 minutes, and this linear decrease can be called bubble's nucleation field which is the estimation of foaming agent. 5 minutes later, nucleation energy is surpassed which suggests that the bubble expansion phenomenon has a parabolic augmentation. In 70/30 ratio, it has a linear decrease of bubble expansion from the baseline to 3 minutes, and this linear decrease can be called bubble's nucleation field. Then, it increases until 70 minutes, and becomes stable. In 80/20 ratio, it has a linear decrease of bubble expansion from the baseline to 2 minutes, and this linear decrease can be called bubble's nucleation field. Then, it increases to 40 minutes, and becomes stable between 40 minutes and 55 minutes. Lastly, it decreases slowly.

The experimental part of this study, which includes the explanation of experimental procedures used in preparing the aqueous slurries, and the measurement of their expansion behavior, helps to find correlations with the mathematical modeling. In experimental study, slurry preparation and presentation of experimental study are described in the prior section as shown in Figure 3.3 to 3.6. In the 50/50 ratio, two experimental studies are presented as shown in Figure 3.3. In this study, experimental studies are consistent. They increase until 25 minutes linearly, and become stable between 25 and 40 minutes. Then they decrease slowly. In the 70/30 ratio, two experimental studies are presented which are in Figure 3.4. In this study, experimental studies are consistent. They increase until 10 minutes linearly, are stable between 10 and 25 minutes, and decrease until 80 minutes. In the 80/20 ratio, two experimental studies are done which are shown in Figure 3.3. In this study, experimental studies are consistent. They increase sharply until 10 minutes and then they are stable, but after 55 minutes they decrease slowly.

The third bubble expansion phenomenon, which is recorded with a camera, is shown in Figure 3.7 where the slurry is placed in a clear plexiglass tube. In the 50/50 ratio, it increases until 10 minutes linearly, and is stable between 10 and 20 minutes. Then it decreases slowly. In the 70/30 ratio, it increases until 3 minutes rapidly, and is stable between 3 and 30 minutes. Then, it increases rapidly. Lastly, it decreases between 35 minutes and 80 minutes. In the 80/20 ratio, it increases until minute rapidly, and increases slowly between 1 minute and 20 minutes. Then, it is stable until 25 minutes. Lastly, it decreases until 80 minutes.

According to mathematical modeling and experimental study of bubble expansion phenomenon, 50/50 ratio increases until 5 minutes slowly in the experimental trial. This increase is called nucleation field. 5 minutes later, it increases rapidly, which is called the baseline of parabolic system in the mathematical modeling, to 25 minutes in the experimentally. 25 minutes later, it is stable until 40 minutes in the experimental trial but in the mathematical modeling, after 25 minutes, it increases slowly until 65 minutes. 40 minutes later, it decreases slowly until 80 minutes in the experimental trial but in the mathematical modeling, after 65 minutes, it is stable until 80 minutes.

In the mathematical modeling and experimental study of bubble expansion phenomenon, 70/30 ratio increases until 3 minutes slowly in the experimental trial. This increase is called nucleation field which lasts until 3 minutes for mathematical modeling. 3 minutes later, it increases rapidly, which is called the baseline of parabolic

system in the mathematical modeling, until 10 minutes in the experimental study. 10 minutes later, it is stable until 25 minutes in the experimental study but in the mathematical modeling, after 10 minutes, it increases slowly until 70 minutes. 25 minutes later, it decreases slowly until 80 minutes in the experimental study but in the mathematical modeling, after 70 minutes, it is stable until 80 minutes.

According to mathematical modeling and experimental study of bubble expansion phenomenon, 80/20 ratio increases until 2 minutes slowly in the experimental study. This increase is called nucleation field which lasts until 2 minutes for mathematical modeling. 2 minutes later, it increases rapidly, which is called at the beginning of parabolic system in the mathematical modeling, until 10 minutes in the experimental study. 10 minutes later, it is stable until 55 minutes in the experimental study but in the mathematical modeling, after 10 minutes, it increases slowly until 40 minutes. 55 minutes later, it decreases slowly until 80 minutes in the experimental study but in the mathematical modeling, after 40 minutes, it decreases slowly until 80 minutes.

In the mathematical modeling and experimental study of bubble expansion phenomenon, different aluminum and calcium hydroxide ratios alter bubble growth for pore formation. Bubble expansion phenomenon has nucleation field at the beginning, and bubble expands rapidly after sufficient waiting time. Then it remains still which is called the stable area of bubble growth for pore formation. Lastly, it decreases slowly.

CHAPTER 5

CONCLUSION AND SUGGESTIONS FUTURE STUDIES

One of the fundamental driving forces governing bubble growth depends on the pressure difference between the inside and outside pressure of a spherical cavity. Numerous studies have been conducted based on this mechanism in order to define the models governing pore formation and growth. According to mathematical modeling, bubble expansion rate depends on the pressure difference between the inside and outside pressure which was shown to depend on six different parameters. These parameters are ultimately considered to have a direct effect on bubble expansion. This theoretical approach is used to find possible correlations between the empirical hydrogen gas release equations developed from the three different aluminum and calcium hydroxide ratios. When calcium hydroxide ratio decreases, the bubble expansion rate decreases due to the nucleation field which was shown in Figure 2.3 to 2.5. ΔP is related with the derivation of bubble radius in equation (2.33) where viscosity is a very significant parameter which controls the bubble expansion rate.

Experimental study includes explanation of the experimental procedures used in preparing the aqueous slurries, and the measurement of their expansion behavior. Aluminum reacts with calcium hydroxide which provides information about the bubble expansion rate. When calcium hydroxide ratio decreases, bubble expansion rate also decreases because of equation (2.28). Hydration of aluminum powder mainly involves the release of hydrogen gas following the equations (2.25) to (2.27). There are three different aluminum and calcium hydroxide ratios which are explained in section 2.2.1. In the 50/50 ratio, slurry preparation rate is 1. In the 70/30 ratio, slurry preparation rate is 6.5 and in the 80/20 ratio, slurry preparation rate is 11. Maximum volume expansion percentages are 250%, 200% and 160% for 50/50, 70/30 and 80/20, respectively as shown in Figure 3.6. While aluminum ratio increases, bubble growth for pore formation rate decreases due to release of hydrogen gases which affects the bubble expansion phenomenon. In the experimental and mathematical modeling, 50/50 ratio has maximum bubble growth rate as compared to 70/30 and 80/20.Viscosity is a significant parameter for experimental modeling.

The study explains the pore mechanism which is formed by the foaming of the glass powder at room temperature as a result of the reaction to be used as thermal insulation in the building sector. Fundamental material is based on glass powder for bubble expansion phenomenon. Glass powder is fly ash in the environment, and it has some advantages such as being free and easily accessible. Other materials that are found freely are basalt or perlite which can be used for bubble growth in pore formation. Basalt or perlite can be used for future studies and their effect can be examined for mathematical and experimental modeling. When other fly ash materials are used to explain bubble expansion phenomenon, this mathematical modeling and experimental study can be applicable for other fly ash materials in the future studies.

.

REFERENCES

Askeland, D., & Phule, P. (2006). *The Science and Engineering of Materials Fifth Edition.* Canada: Thomson.

Gent, A., & Tompkins, D. (1969). Surface Energy Effects for Small Holes or Particles in Elastomers. *Journal of Polymer Science Part A-2 Volume 7*, 1483-1488.

Hamad, A. J. (2014). Materials, Production, Properties and Application of Aerated Light-weight Concrete. *International Journal of Materials Science and Engineering Vol. 2, No. 2*, 152-157.

Kanehira, S., Kanamori, S., Nagashima, K., Saeki, T., Visbal, H., Fukui, T., et al. (2013). Controllable Hydrogen Release via Aluminum Powder Corrosion in Calciumhydroxide Solutions. *Journal of Asian Ceramic Societies*, 296-303.

Liu, P., & Chen, G. (First Edition 2014). *Porous Materials Processing and Applications.* USA: Elsevier.

Liyun, W. (1998). Foam Glass Production Technology and Economic Discussions. *Beijing University of Technology*, 115-117.

Rafalowski, M. (2003). *Fly Ash Facts for Highway Engineers.* USA: American Coal Ash Association.

Scheffler, M., & Colombo, P. (2005). *Cellular Ceramics.* Germany: Wiley Publishers.

Schwartzberg, H., Wu, J., Nussinovitch, A., & Mugerwa, J. (1995). Modelling Deformation and Flow During Vapor Induced Pufing. *Elsevier* , 329-372.

Steiner, A. (2006). *Foam Glass Production From Vitrified Municipal Waste Fly Ashes.* Netherlands: Eindhoven university Press.

Vargaftik, N., Volkov, B., & Voljak, L. (1983). International Tables of the Surface Tension of Water. *Journal of Physical and Chemical Reference Data*, 817.

Wang, L., Ganjyal, G., Jones, D., Weller, C., & Hanna, M. (2005). Modeling of Bubble Growth Dynamics and Nonisothermal Expansion in Starch-Based Foams During Extrusion. *Advances in Polymer Technology*, 29-45.

Xiaoping, F., Zhifeng, M., Jiahua, Z., & Hong, X. (2011). Analysis of Starch Bubble Breakage during Extrusion Expansion by Finite Elements Method. *Advanced Materials Research*, 2449-2459.

Yang, W., & Yeh, H. (1966). Theoretical Study of Bubble Dynamics in Purely Viscous Fluids. *A.I.Ch.E. Journal Vol. 12, No. 5*, 927-931.

APPENDIX A

CALCULATION OF MATHEMATICAL MODELING SYSTEM

According to linear system equation;

If $A(x_1, y_1)$ and $B(x_2, y_2)$ are known;

$$\frac{y_2-y_1}{x_2-x_1} = \frac{y-y_2}{x-x_2} \tag{A.1}$$

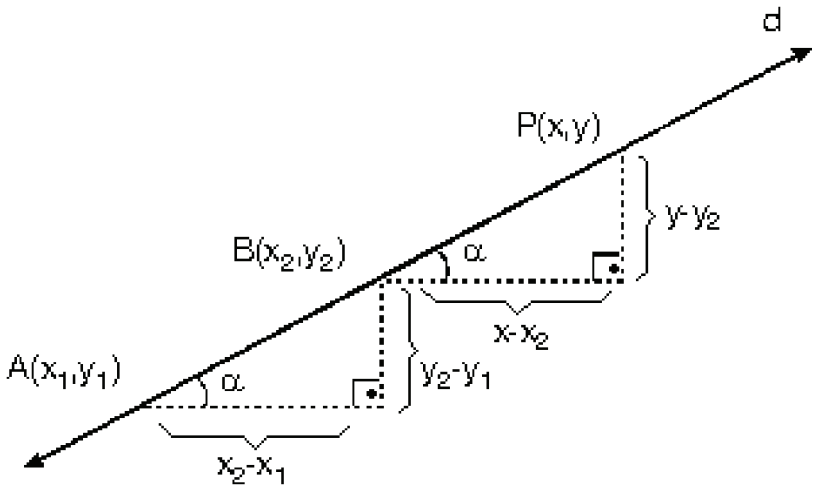

Figure A.1. Linear system

According to parabolic system;

$$f(x) = ax^2 + bx + c$$

$$T(r, k)$$

$$r = -\frac{b}{2a} \tag{A.2}$$

$$k = f(r) = \frac{4ac-b^2}{4a} \tag{A.3}$$

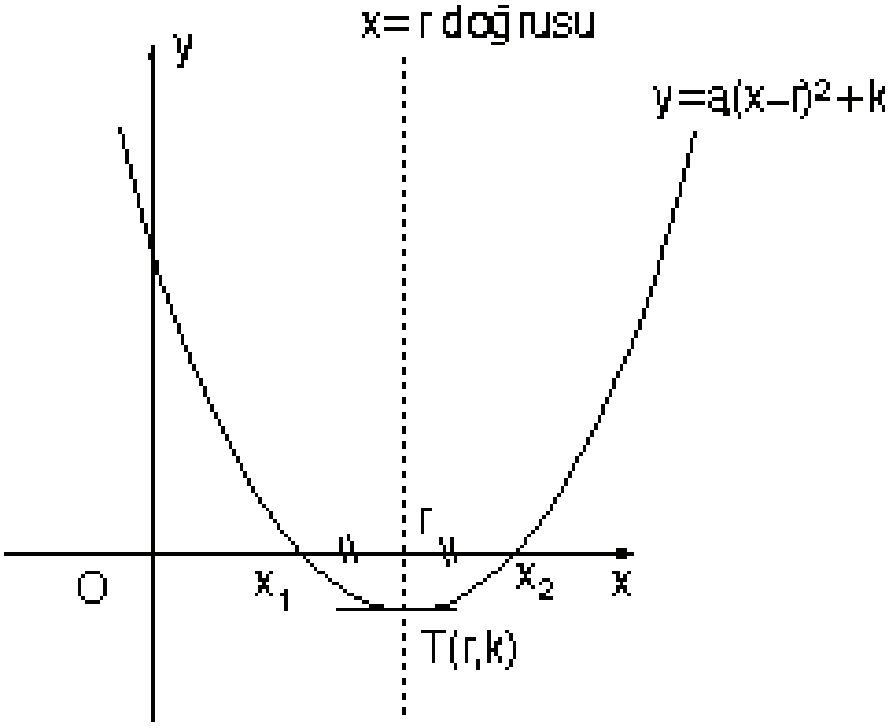

Figure A.2. Parabolic system

All reactions are described with these parts that are explained below;

According to 50/50;

First part is (0,0) – (20,4.5).

$$\frac{4.5-0}{20-0}=\frac{y-4.5}{x-20}$$

$$9x=4y$$

$$9t=40\left(\frac{4}{3}\pi rR^3\right)$$

$$R=\left(\frac{27}{160\pi}t\right)^{1/3} \quad (A.4)$$

Second part is (20,4.5) – (45,6).

$$y = ax^2 + bx + c$$

$$T(r,k) = T(20,4,5)$$

$$y = a(x - r)^2 + k$$

$$6 = a(45 - 14)^2 + 4.5 \quad \Rightarrow \quad a = 0.0024$$

$$y = 0.0024(t - 14)^2 + 4.5$$

$$\frac{4}{3}\pi R^3 = 0.0024(t - 14)^2 + 4{,}5$$

$$R = (0.005(t - 14)^2 + 1.07)^{1/3} \qquad \text{(A.5)}$$

According to 70/30;

First part is (0,0) – (14,4.5).

$$\frac{4.5 - 0}{14 - 0} = \frac{y - 4.5}{x - 14}$$

$$9x = 28y$$

$$9t = 28\left(\frac{4}{3}\pi r R^3\right)$$

$$R = \left(\frac{27}{112\pi}t\right)^{1/3} \qquad \text{(A.6)}$$

Second part is (14,4.5) – (50,7).

$$y = ax^2 + bx + c$$

$$T(r,k) = T(14,4,5)$$

$$y = a(x - r)^2 + k$$

$$7 = a(50 - 14)^2 + 4.5 \quad \Rightarrow \quad a = 0.0019$$

$$y = 0.0019(t - 14)^2 + 4.5$$

$$\frac{4}{3}\pi R^3 = 0.0019(t-14)^2 + 4.5$$

$$R = (0.004(t-14)^2 + 1.07)^{1/3} \quad \text{(A.7)}$$

According to 80/20;

First part is (0,0) – (8,3).

$$\frac{3-0}{8-0} = \frac{y-3}{x-8}$$

$$3x = 8y$$

$$3t = 8\left(\frac{4}{3}\pi r R^3\right)$$

$$R = \left(\frac{9}{32\pi}t\right)^{1/3} \quad \text{(A.8)}$$

Second part is (8,3) – (40,9.5).

$$y = ax^2 + bx + c$$

$$T(r,k) = T(8,3)$$

$$y = a(x-r)^2 + k$$

$$9.5 = a(40-8)^2 + 3 \quad \Rightarrow \quad a = 0.006$$

$$y = 0.006(t-8)^2 + 3$$

$$\frac{4}{3}\pi R^3 = 0.006(t-8)^2 + 3$$

$$R = (0.001(t-8)^2 + 0.71)^{1/3} \quad \text{(A.9)}$$

APPENDIX B

RESULTS OF EXPERIMENTAL STUDY

Firstly, 50/50 experiment shows us,

Figure B.1.a. 50/50 at the beginning

At the beginning, bubble expansion's height is 22 millimeters. 5 minutes later,

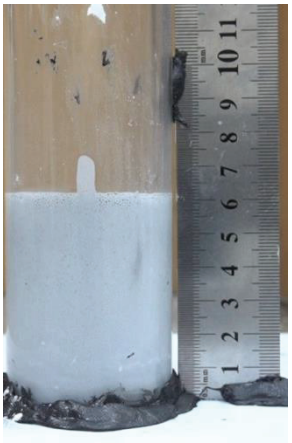

Figure B.1.b. 50/50 (5 minutes later)

5 minutes later, bubble expansion's height is 60 millimeters. 10 minutes later,

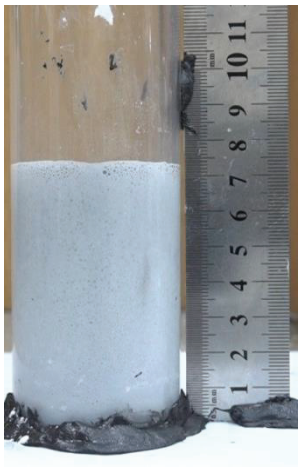

Figure B.1.c. 50/50 (10 minutes later)

10 minutes later, bubble expansion’s height is 73 millimeters. 15 minutes later,

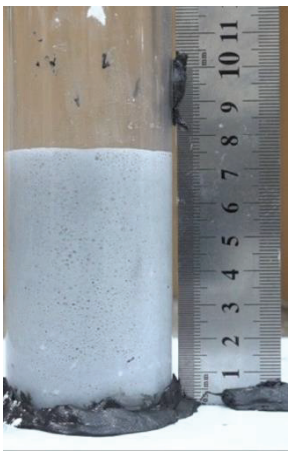

Figure B.1.d. 50/50 (15 minutes later)

15 minutes later, bubble expansion’s height is 75 millimeters. 20 minutes later,

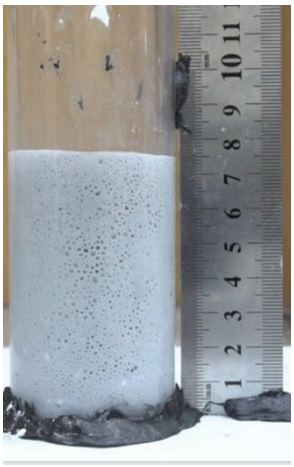

Figure B.1.e. 50/50 (20 minutes later)

20 minutes later, bubble expansion’s height is 75 millimeters. 25 minutes later,

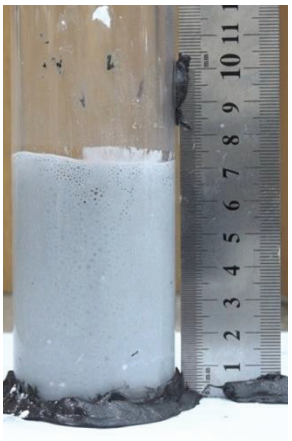

Figure B.1.f. 50/50 (25 minutes later)

25 minutes later, bubble expansion’s height is 73 millimeters. 30 minutes later,

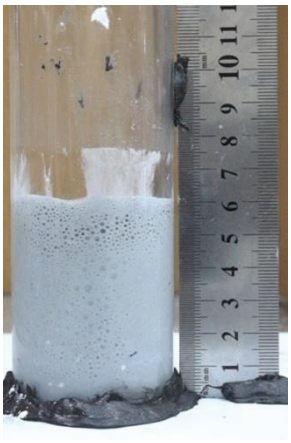

Figure B.1.g. 50/50 (30 minutes later)

30 minutes later, bubble expansion’s height is 60 millimeters. 40 minutes later,

Figure B.1.h. 50/50 (40 minutes later)

40 minutes later, bubble expansion’s height is 40 millimeters. 50 minutes later,

Figure B.1.i. 50/50 (50 minutes later)

50 minutes later, bubble expansion’s height is 30 millimeters. 60 minutes later,

Figure B.1.j. 50/50 (60 minutes later)

60 minutes later, bubble expansion’s height is 25 millimeters. 70 minutes later,

Figure B.1.k. 50/50 (70 minutes later)

70 minutes later, bubble expansion’s height is 25 millimeters. 80 minutes later,

Figure B.1.l. 50/50 (80 minutes later)

80 minutes later, bubble expansion’s height is 25 millimeters.

Secondly, 70/30 experiment shows us,

Figure B.2.a. 70/30 at the beginning

At the beginning, bubble expansion’s height is 22 millimeters. 5 minutes later,

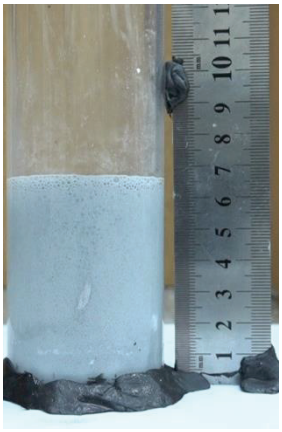

Figure B.2.b. 70/30 (5 minutes later)

5 minutes later, bubble expansion’s height is 65 millimeters. 10 minutes later,

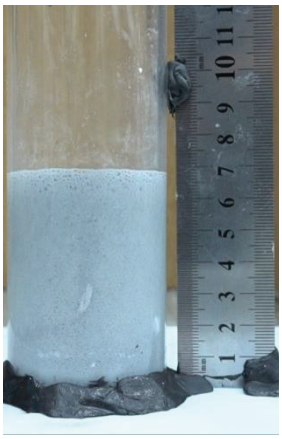

Figure B.2.c. 70/30 (10 minutes later)

10 minutes later, bubble expansion’s height is 68 millimeters. 15 minutes later,

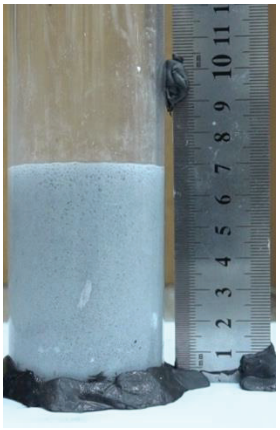

Figure B.2.d. 70/30 (15 minutes later)

15 minutes later, bubble expansion’s height is 70 millimeters. 20 minutes later,

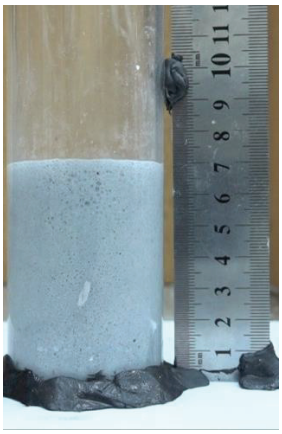

Figure B.2.e. 70/30 (20 minutes later)

20 minutes later, bubble expansion’s height is 70 millimeters. 25 minutes later,

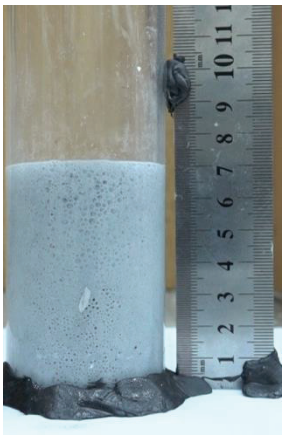

Figure B.2.f. 70/30 (25 minutes later)

25 minutes later, bubble expansion’s height is 70 millimeters. 30 minutes later,

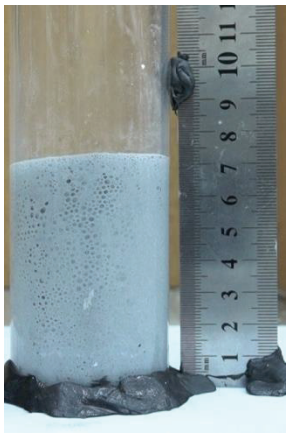

Figure B.2.g. 70/30 (30 minutes later)

30 minutes later, bubble expansion’s height is 72 millimeters. 40 minutes later,

Figure B.2.h. 70/30 (40 minutes later)

40 minutes later, bubble expansion’s height is 60 millimeters. 50 minutes later,

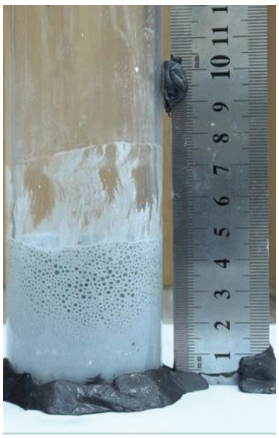

Figure B.2.i. 70/30 (50 minutes later)

50 minutes later, bubble expansion’s height is 45 millimeters. 60 minutes later,

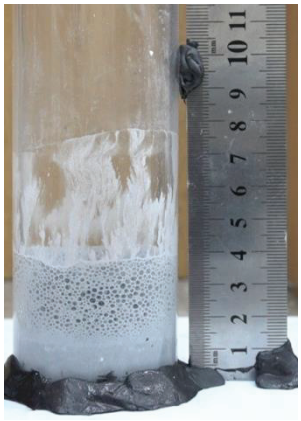

Figure B.2.j. 70/30 (60 minutes later)

60 minutes later, bubble expansion’s height is 40 millimeters. 70 minutes later,

Figure B.2.k. 70/30 (70 minutes later)

70 minutes later, bubble expansion’s height is 30 millimeters. 80 minutes later,

Figure B.2.l. 70/30 (70 minutes later)

80 minutes later, bubble expansion’s height is 25 millimeters.

Lastly, 80/20 experiment shows us,

Figure B.3.a. 80/20 at the beginning

At the beginning, bubble expansion’s height is 22 millimeters. 5 minutes later,

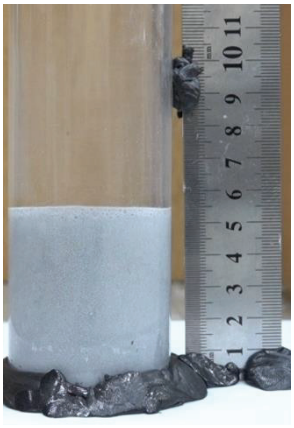

Figure B.3.b. 80/20 (5 minutes later)

5 minutes later, bubble expansion’s height is 55 millimeters. 10 minutes later,

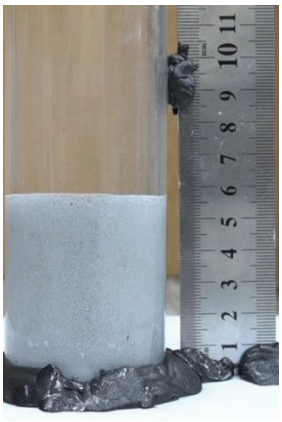

Figure B.3.c. 80/20 (10 minutes later)

10 minutes later, bubble expansion’s height is 57 millimeters. 15 minutes later,

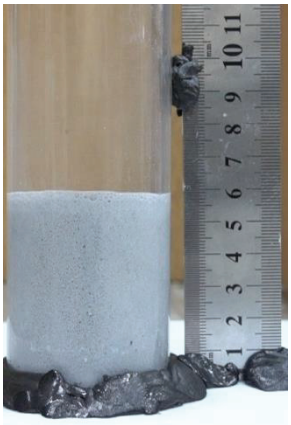

Figure B.3.d. 80/20 (15 minutes later)

15 minutes later, bubble expansion’s height is 59 millimeters. 20 minutes later,

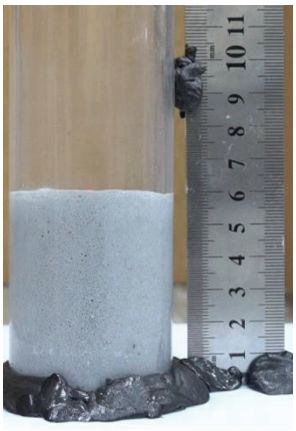

Figure B.3.e. 80/20 (20 minutes later)

20 minutes later, bubble expansion’s height is 60 millimeters. 25 minutes later,

Figure B.3.f. 80/20 (25 minutes later)

25 minutes later, bubble expansion’s height is 60 millimeters. 30 minutes later,

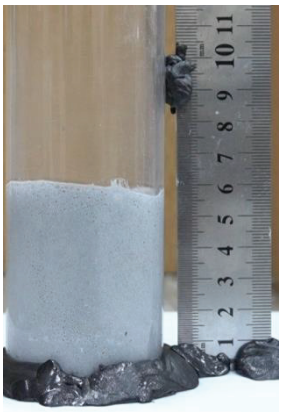

Figure B.3.g. 80/20 (30 minutes later)

30 minutes later, bubble expansion’s height is 58 millimeters. 40 minutes later,

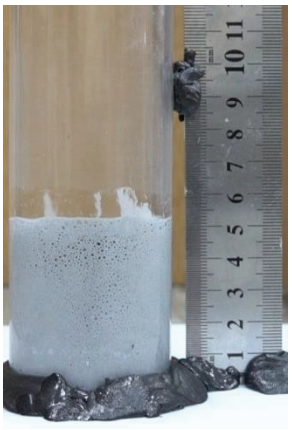

Figure B.3.h. 80/20 (40 minutes later)

40 minutes later, bubble expansion’s height is 53 millimeters. 50 minutes later,

Figure B.3.i. 80/20 (50 minutes later)

50 minutes later, bubble expansion’s height is 45 millimeters. 60 minutes later,

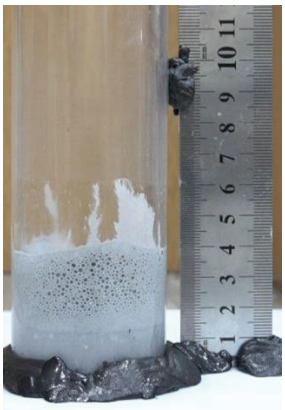

Figure B.3.j. 80/20 (60 minutes later)

60 minutes later, bubble expansion’s height is 40 millimeters. 70 minutes later,

Figure B.3.k. 80/20 (70 minutes later)

70 minutes later, bubble expansion’s height is 38 millimeters. 80 minutes later,

Figure B.3.l. 80/20 (80 minutes later)

80 minutes later, bubble expansion’s height is 35 millimeters.